THE JOURNAL OF BIOLOGICAL CHEMISTRY VOL. 290, NO. 30, pp. 18621–18635, July 24, 2015

Co-chaperone Specificity in Gating of the Polypeptide Conducting Channel in the Membrane of the Human Endoplasmic Reticulum*

Received for publication, January 6, 2015, and in revised form, May 20, 2015 Published, JBC Papers in Press, June 17, 2015, DOI 10.1074/jbc.M115.636639

Stefan Schorr[‡], Marie-Christine Klein[‡], Igor Gamayun[§], Armin Melnyk[‡], Martin Jung[‡], Nico Schäuble[‡], Qian Wang[¶], Birgit Hemmis[‖], Florian Bochen[‡], Markus Greiner[‡], Pavel Lampel[‡], Sabine Katharina Urban[‡], Sarah Hassdenteufel[‡], Johanna Dudek[‡], Xing-Zhen Chen[¶], Richard Wagner[‖], Adolfo Cavalié[§], and Richard Zimmermann[‡1]

From the Departments of [‡]Medical Biochemistry and Molecular Biology and [§]Experimental and Clinical Pharmacology and Toxicology, Saarland University, 66421 Homburg, Germany, the [¶]Department of Physiology, University of Alberta, Edmonton T6G 2H7, Canada, and the [‖]Division of Biophysics, Universität Osnabrück, FB Biologie/Chemie, 49076 Osnabrück, Germany

Background: The molecular chaperone immunoglobulin heavy-chain-binding protein (BiP) modulates gating of the polypeptide-conducting and calcium-permeable channel (Sec61 complex) in the membrane of the endoplasmic reticulum (ER).
Results: Two co-chaperones, ERj3 and ERj6, support BiP in preventing ER calcium leakage via Sec61 complex.
Conclusion: ERj3 and ERj6 facilitate Sec61 channel closing.
Significance: Different co-chaperones assist BiP in Sec61 channel gating.

In mammalian cells, signal peptide-dependent protein transport into the endoplasmic reticulum (ER) is mediated by a dynamic polypeptide-conducting channel, the heterotrimeric Sec61 complex. Previous work has characterized the Sec61 complex as a potential ER Ca^{2+} leak channel in HeLa cells and identified ER lumenal molecular chaperone immunoglobulin heavy-chain-binding protein (BiP) as limiting Ca^{2+} leakage via the open Sec61 channel by facilitating channel closing. This BiP activity involves binding of BiP to the ER lumenal loop 7 of Sec61α in the vicinity of tyrosine 344. Of note, the Y344H mutation destroys the BiP binding site and causes pancreatic β-cell apoptosis and diabetes in mice. Here, we systematically depleted HeLa cells of the BiP co-chaperones by siRNA-mediated gene silencing and used live cell Ca^{2+} imaging to monitor the effects on ER Ca^{2+} leakage. Depletion of either one of the ER lumenal BiP co-chaperones, ERj3 and ERj6, but not the ER membrane-resident co-chaperones (such as Sec63 protein, which assists BiP in Sec61 channel opening) led to increased Ca^{2+} leakage via Sec6 complex, thereby phenocopying the effect of BiP depletion. Thus, BiP facilitates Sec61 channel closure (*i.e.* limits ER Ca^{2+} leakage) via the Sec61 channel with the help of ERj3 and ERj6. Interestingly, deletion of ERj6 causes pancreatic β-cell failure and diabetes in mice and humans. We suggest that co-chaperone-controlled gating of the Sec61 channel by BiP is particularly important for cells, which are highly active in protein secretion, and that breakdown of this regulatory mechanism can cause apoptosis and disease.

In mammalian cells, the endoplasmic reticulum (ER)[2] is central to protein biogenesis as well as calcium (Ca^{2+}) homeostasis (1–4). The protein biogenesis function involves an aqueous polypeptide-conducting pore in the ER membrane, which is formed by the heterotrimeric Sec61 complex (5–11); the store- and receptor-controlled Ca^{2+} release function requires a steep ER to cytosol gradient, with 500–800 μM free Ca^{2+} in the ER. Recent work demonstrated that the Sec61 complex can transiently allow passive ER Ca^{2+} efflux (11–14). Therefore, gating of the Sec61 channel has to be tightly regulated by its allosteric effectors, ER lumenal immunoglobulin heavy-chain-binding protein (BiP) and cytosolic Ca^{2+}-calmodulin (CaM). In addition, the sarcoplasmic/endoplasmic reticulum calcium ATPase (SERCA) counteracts Ca^{2+} leakage from the ER (15).

The Hsp70-type molecular chaperone BiP plays a role in Sec61 channel closure (8, 9, 16, 17) (Fig. 1). By combining siRNA-mediated gene silencing and live cell Ca^{2+} imaging, it was observed in HeLa cells that reduced levels of BiP lead to increased Ca^{2+} leakage from the ER via the Sec61 complex. This increased leakage was seen in imaging of both cytosolic and ER lumenal Ca^{2+} when cells were challenged with thapsigargin in the presence of extracellular EGTA (16). Furthermore, we found that BiP binds to loop 7 of Sec61α in order to facilitate Sec61 channel closure. The action of BiP was highly specific (*i.e.* it could not be compensated by other abundant ER lumenal chaperones (PDI, Grp94, or calreticulin) or even its yeast ortholog, Kar2p) (16). Strikingly, mutant variant BiPR197E, which is deficient in its ability to cooperate with Hsp40-type co-chaperones, was also unable to mediate Sec61 channel closure, pointing toward the involvement of an Hsp40-type co-chaperone in Sec61 channel closure (16). Furthermore, it was shown with a similar experimental approach that Ca^{2+}-CaM can bind to an IQ motif present in the cytosolic amino terminus of the α-subunit of the hetero-

* This work was supported by Deutsche Forschungsgemeinschaft Grants FOR 967, IRTG 1830, and SFB 894 and by a HOMFOR grant (to M. J.). The authors declare that they have no conflicts of interest with the contents of this article.
[1] To whom correspondence should be addressed. Tel.: 49-6841-1626510; Fax: 49-6841-1626288; E-mail: richard.zimmermann@uks.eu.
[2] The abbreviations used are: ER, endoplasmic reticulum; BiP, immunoglobulin heavy-chain-binding protein; CaM, calmodulin; Hsp, heat shock protein; SERCA, sarcoplasmic/endoplasmic reticulum calcium ATPase; SIM, structured illumination microscopy; POD, peroxidase; CFP, cyan fluorescent protein; RM, rough microsomes; PKRM, puromycin and high salt treated RM.

trimeric Sec61 complex and, with the help of ER membrane protein Sec62, limit Ca^{2+} leakage from the ER after Ca^{2+} has started to leak out (13, 18).

Of note, a mouse model for diabetes has indicated that a single amino acid exchange in the ER lumenal loop 7 of murine Sec61α leads to a partially deficient Sec61 complex and to β-cell death as well as diabetes (19). When wild type Sec61α was replaced with the corresponding mutant Sec61αY344H in human cells, Ca^{2+} leakage from the ER was increased and was no longer affected by manipulation of the BiP concentration (16). Therefore, it was suggested that failure of BiP to facilitate Sec61 channel closure in the homozygous *SEC61A1Y344H* mouse contributes to apoptosis of cells with high secretory activity, such as pancreatic β-cells. It is interesting to note that various other mutations and knockouts of resident ER proteins can cause diabetes in mice, such as deletion of the Hsp40-type co-chaperones of BiP ERj4 and ERj6 (20, 21) or of the BiP-interacting protein PKR-like kinase (22). However, diabetes can also be caused in humans and mice by mutations in genes coding for non-ER proteins, such as the insulin gene.

We asked whether the Hsp40-type co-chaperones of BiP that are involved in Sec61 channel closure can be identified and whether the mechanism of Sec61 channel closure by BiP can be further elucidated. For the latter question, we addressed the questions of whether artificial ligands of Sec61α loop 7 (*i.e.* specific antibodies or Fab fragments thereof) can substitute for BiP in mediating Sec61 channel closure in single channel measurements. We identified ERj3 (also termed DnaJB11) and ERj6 (also termed DnaJC3 or $p58^{IPK}$) as the BiP co-chaperones that are involved in Sec61 channel closure in HeLa cells. Furthermore, we observed that Fabs, directed against Sec61α loop 7, can indeed trigger Sec61 channel closing in single channel recordings. In various tumor cells, inefficient Sec61 channel closure after *SEC62* gene silencing or CaM inhibition is associated with reduced migratory potential (18, 23). In our current study, we observed that *ERJ3* and *ERJ6* silencing causes the similar phenomenon, confirming their significance in the regulation of the Sec61 channel.

Experimental Procedures

Materials—Enhanced chemiluminescence (ECL™), ECL™ Plex goat anti-rabbit IgG-Cy5, and ECL™ Plex goat anti-mouse IgG-Cy3 conjugate were purchased from GE Healthcare. Thapsigargin, ionomycin, and Fura-2 AM were from Invitrogen/Molecular Probes. The nucleic acid gel stain GelRED was from GeneON. Antibodies against ERj5 were from Abnova, antibodies against ERj6 were from Cell Signaling, and antibodies against β-actin were from Sigma. Antibodies against ERj4 were a kind gift from Linda Hendershot (St. Jude's Children's Hospital, Memphis, TN). Antibodies against BiP and GFP for immunoprecipitation were from Santa Cruz Biotechnology, Inc., and antibodies against hexahistidine were from Cell Signaling. Rabbit antibodies were raised against the carboxyl-terminal peptide (14-mer) or loop 7 (12-mer) of human Sec61α; against the carboxyl-terminal peptides of ERj3 (14-mer), Sec62 (11-mer), or Sec63 (13-mer); against the amino-terminal peptides of human BiP (12-mer) or Grp170 (11-mer), all plus an amino- or carboxyl-terminal cysteine; and against ERj1C-ΔN21 (24), respectively. Where indicated, antibodies were affinity-purified on Sulfolink-immobilized peptides (Thermo Fisher Scientific). Fabs were produced from affinity-purified antibodies with the Pierce Fab Preparation Kit (Thermo Fisher Scientific) according to the manufacturer's protocol. GST-tagged ERj proteins and His-tagged BiP from hamsters were purified as described previously (25–28). Fabs were analyzed by reductive or non-reductive (with or without β-mercaptoethanol in the sample buffer) SDS-PAGE.

TABLE 1
siRNAs

Name	Sequence	Source
BIP siRNA	CCUUCGAUGUGUCUCUUCUtt	Qiagen
ERJ1 siRNA	CCUAAUUGGUGGCCAUUUAtt	Qiagen
ERJ2-UTR siRNA	GGGAGGUGUAGUUUUUUUAtt	Qiagen
ERJ3#1 siRNA	CGAAUGCCCUAAUGUCAAAtt	Qiagen
ERJ3#2 siRNA	GGACGAGAUUUCUAUAAGAtt	Qiagen
ERJ3 UTR siRNA	CCUGAGUUUCAAGAAUUAAtt	Qiagen
ERJ5#1 siRNA	CGACGGACUUAUAAUGUUUtt	Qiagen
ERJ5#2 siRNA	GGGCCUAUCCAACUGUUAAtt	Qiagen
ERJ6#1 siRNA	GGAGAACCUAGGAAAGCUAtt	Qiagen
ERJ6#2 siRNA	GAAACGAGAUUAUUAUAAAtt	Qiagen
ERJ7 siRNA	GUCUCAAUUUGAUAGUCUAtt	Qiagen
SEC61A1-UTR siRNA	CACUGAAAUGUCUACGUUUtt	Applied Biosystems

Cell Culture—HeLa cells (ATCC catalog no. CCL-2) were cultivated at 37 °C in Dulbecco's modified Eagle's medium (DMEM) (Gibco) with 10% fetal bovine serum (FBS) (Biochrom) and 1% penicillin/streptomycin (PAA) in a humidified environment with 5% CO_2. For live cell calcium imaging, cells were grown on 25-mm glass coverslips pretreated with poly-L-lysine (1 mg/ml) for 1 h. Cell growth was monitored using the Countess® automated cell counter (Invitrogen) according to the manufacturer's instructions.

A HeLa cell line that stably expresses the FRET-based calcium sensor D1ER (HeLa-D1ER) was generated to measure the lumenal calcium concentration in the ER. D1ER was kindly provided by R. Y. Tsien (29). HeLa-D1ER cells were maintained in culture under selection with G418 (minimal essential medium (Gibco), 10% FBS, 0.5 mg/ml G418) and transferred to poly-L-lysine-coated glass coverslips previous to silencing and live cell calcium imaging experiments, as described below for naive HeLa cells.

Silencing of Gene Expression by siRNA—For gene silencing, 5.2×10^5 HeLa cells were seeded per 6-cm culture plate in normal culture. The cells were transfected with targeting siRNA (Table 1) or control siRNA (AllStars Negative Control siRNA, Qiagen) using HiPerFect Reagent (Qiagen) according to the manufacturer's instructions (typical final concentration of siRNAs was 20 nM). After 24 h, the medium was changed, and the cells were transfected a second time. *SEC61A1* silencing was carried out as described previously (30). Silencing efficiencies were evaluated by Western blot analysis using the respective antibodies and an anti-β-actin-antibody from mice. The primary antibodies were visualized using ECL™ Plex goat anti-rabbit IgG-Cy5 or ECL™ Plex goat anti-mouse IgG-Cy3 conjugate and the Typhoon-Trio imaging system in combination with the ImageQuant TL software version 7.0 (GE Healthcare). Alternatively, signals were detected using a secondary peroxidase (POD)-coupled anti-rabbit antibody (Sigma) and ECL™,

visualized with a Fusion SL (peqlab) luminescence imaging system.

Complementation Analysis—To rescue the phenotype of *ERJ3* silencing, the *ERJ3* cDNA was inserted into the multicloning sites of a pCDNA3-IRES-GFP vector. Cells were treated with *ERJ3*-UTR siRNA as described above for 48 h. Subsequently, control siRNA- and *ERJ3* siRNA-treated cells were transfected with either vector or *ERJ3* expression plasmid using Fugene HD (Promega) according to the manufacturer's instructions.

Real-time Cell Proliferation Analysis—The xCELLigence SP system (Roche Applied Science) was used for the real-time analysis of cell proliferation. In this system, 5.0×10^3 HeLa cells treated with control siRNA or siRNAs against *ERJ3* and *ERJ6*, respectively, for 48 h were seeded into a 96-well E-plate (Roche Applied Science) according to the manufacturer's instructions. Cell proliferation was monitored for 48 h, and the data were evaluated with RTCA version 2.0 software (Roche Applied Science).

Quantitative Real-time PCR Analysis—Cells were harvested, and total RNA was isolated by using the RNA blood kit (Qiagen). Reverse transcription was performed with Superscript II RT (Invitrogen) and olgigo(dT) primers (Eurofins Genomics), and the cDNA was purified using the PCR purification kit (Qiagen). TaqMan® gene expression assays (Applied Biosystems) were used for quantitative real-time PCR of *SEC61A1* (Hs00273698_m1), *ERJ3* (Hs00212527_m1), *ERJ4* (Hs00202448_m1), *ERJ6* (Hs00534483_m1), *CHOP* (Hs99999174_m1), and *BIP* (Hs99999174_m1) in a StepOne Plus 96-well system (Applied Biosystems). ΔCt values were calculated using *ACTB* (Hs00357333_m1) as a standard, and the values were then normalized to control siRNA-treated cells.

Alternatively, *XBP1* was amplified in the same cDNA with *Pfu* polymerase (Thermo Fisher Scientific) and established primers (CACCTGAGCCCCGAGGAG and TTAGTTCATTAATGGCTTCCAGC) (31). The PCR products were subjected to gel electrophoresis in the presence of GelRED and visualized with the GelDoc XR imaging system (Bio-Rad).

Three-dimensional Structured Illumination Microscopy—Cells were seeded on glass coverslips and treated as indicated. After 96 h, the glass slides were removed and washed twice with cold PBS. Cells were fixed with 4% paraformaldehyde for 20 min at 4 °C. Fixed cells were permeabilized and blocked with PSS (PBS plus 0.1% saponin and 10% FCS) for 1 h at room temperature. To improve the antigen accessibility, RNase A (Roche Applied Science) was added to a final concentration of 50 μg/ml. After washing with PSS, indirect immunofluorescence staining with an affinity-purified rabbit antipeptide antibody directed against the COOH-terminal undecapeptide of human Sec62 protein (plus an amino-terminal cysteine) and Alexa Fluor 594-coupled secondary antibody from goats (Invitrogen) was performed. We note that the anti-Sec62 antibody is specific for Sec62 under denaturing as well as native conditions (*i.e.* Western blot and fluorescence microscopy signals were quenched after silencing of the *SEC62* gene) (22). Cells were analyzed by microscopy on an Elyra SIM PS1 (Carl Zeiss-MicroImaging). The microscope was equipped with a plan-apochromat oil differential interference contrast lens with ×63 magnification and 1.4 numerical aperture (Carl Zeiss) and an iXon^{EM}+885 EMCCD camera (Andor Technology). The mounting medium was Roti®-Mount FluorCare DAPI (Carl Roth), and the oil was Immersol 518F (Carl Zeiss).

Protein Transport into Semipermeabilized Cells—Precursor polypeptides were synthesized in reticulocyte lysate (nuclease-treated; Promega) in the presence of [^{35}S]methionine (PerkinElmer Life Sciences) plus buffer or semipermeabilized cells, resulting in a final concentration between 3,200 and 12,800 cell equivalents/μl, for 60 min at 30 °C (co-translational transport experiment) (32, 33). Of note, the respective membrane concentration was in the linear range for the assay. Alternatively, precursor polypeptides were synthesized in reticulocyte lysate in the presence of [^{35}S]methionine for 16 min at 30 °C. After 5 min of incubation with RNase A (final concentration, 80 μg/ml) and cycloheximide (final concentration, 100 μg/ml) at 30 °C, buffer or semipermeabilized cells, resulting in a final concentration of 12,800 cell equivalents/μl, were added, and the incubation was continued for 30 min (post-translational transport experiment). The cells had previously been treated with targeting or control siRNA for 96 h. Semipermeabilized cells were prepared by digitonin treatment from identical cell numbers according to a published procedure (32, 33). Their concentrations were adjusted according to A_{280} in 2% SDS and eventually confirmed by SDS-PAGE and protein staining. All samples were analyzed by SDS-PAGE and phosphorimaging (Typhoon-Trio imaging system). ImageQuant TL software version 7.0 was used for quantifications. Silencing efficiency was evaluated by Western blot.

Live Cell Calcium Imaging—Live cell calcium imaging for cytosolic Ca^{2+} was carried out as described previously (14, 30, 34, 35). HeLa cells were loaded with 4 μM Fura-2 AM in DMEM for 45 min at 25 °C. Cells were washed twice and incubated in a calcium-free buffer (140 mM NaCl, 5 mM KCl, 1 mM $MgCl_2$, 0.5 mM EGTA, 10 mM glucose in 10 mM HEPES-KOH, pH 7.35) at room temperature. During the experiment, cells were treated with thapsigargin (1 μM), and ratiometric measurements were carried out for 7.5 or 12.5 min. Where indicated, HeLa cells were treated with siRNA for 96 h prior to calcium imaging. Data were collected on an iMIC microscope and the polychromator V (Till Photonics) by alternate excitation at 340 and 380 nm and measurement of the emitted fluorescence at 510 nm. The microscope was equipped with a Fluar M27 lens with ×20 magnification and 0.75 numerical aperture (Carl Zeiss) and an iXon^{EM}+ camera (Andor Technology). Images containing 50–55 cells/frame were sampled every 3 s using TILLvisION software (Till Photonics). Fura-2 signals were recorded as the ratios F_{340}/F_{380}, where F_{340} and F_{380} correspond to the background-subtracted fluorescence intensity at 340 and 380 nm, respectively. Cytosolic [Ca^{2+}] was estimated from ratio measurements using an established calibration method (36). Data were analyzed using Excel 2007. p values were determined by unpaired t tests. Alternatively, HeLa cells were loaded with 4 μM Fura-2 AM and washed and incubated in the calcium-free buffer. After ratiometric measurements were carried out for 1

min, ionomycin (5 μM) was added, and the measurements continued. Data were collected on the iMIC microscope.

The lumenal calcium concentration in ER ($[Ca^{2+}]_{ER}$) was analyzed using the FRET-based calcium sensor D1ER, which comprises two fluorescent proteins, CFP and citrine, and two sensing proteins, calmodulin and a calmodulin-binding peptide derived from skeletal muscle myosin light chain kinase (29). D1ER was stably expressed in the HeLa-D1ER cell line (see "Cell Culture"). The experiments were carried out with the iMIC microscope, the polychromator V, and the Live Acquisition software (Till Photonics). HeLa-D1ER cells were exposed to 433 nm, and the emitted florescence was split at 469/23 nm and 536/27 nm to obtain the CFP and citrine components, respectively. The cell fluorescence was additionally passed through a dichrotome and projected on the chip of the microscope camera to obtain simultaneous CFP and citrine images. Image pairs containing 10–15 cells/frame were obtained at ×20 magnification every 10 s. The FRET ratios were calculated from background-subtracted CFP and citrine image pairs as F_{536}/F_{469}, were F_{536} and F_{469} represent the citrine and CFP fluorescence intensities, respectively (29). In order to measure $[Ca^{2+}]_{ER}$ and $[Ca^{2+}]_{cytosol}$ simultaneously in the same cell, HeLa-D1ER cells were loaded with Fura-2 AM and incubated in a calcium-free buffer as described for naive HeLa cells. Fura-2 signals were recorded and analyzed as described for naive HeLa cells. To allow the recording of D1ER and Fura-2 signals in the same cells, the filter sets were automatically exchanged in such a way that two pairs of images were obtained every 10 s. The ratios F_{536}/F_{469} and F_{340}/F_{380}, which reflect $[Ca^{2+}]_{ER}$ and $[Ca^{2+}]_{cytosol}$, respectively, were measured in each image pair.

Surface Plasmon Resonance Spectroscopy—Surface plasmon resonance spectroscopy was performed in a BIAlite upgrade system (BIACORE) according to our established procedure (25–28). Monoclonal goat anti-GST antibodies were immobilized on a sensor chip CM5 (BIACORE). GST hybrid proteins were bound to the immobilized antibodies in the measuring cell; GST was bound to the antibodies in the reference cell. For interaction analysis, the chip was equilibrated with running buffer (150 mM NaCl, 3 mM KCl, 1 mM $MgCl_2$, 0.1% Tween 20, 1 mM ATP in sodium phosphate, pH 7.4) at a flow rate of 5 μl/min. Subsequently, solutions containing increasing concentrations of BiP were passed over the chip surface. Each application was followed by application of running buffer and eventually with running buffer that was supplemented with high salt. The analysis was carried out by employing BIA evaluation software version 2.2.4 (BIACORE).

Peptides corresponding to the peptides used for generation of the loop 7 (residues 339–353) antibodies were synthesized with biotinylated dipeptide KG at the carboxyl terminus and immobilized in the measuring cell of Biacore avidin sensor chip SA. The reference cell was loaded with carboxyl-terminally biotinylated Sec61α peptide (residues 325–339 with biotinylated dipeptide KG). The running buffer was 10 mM HEPES/KOH (pH 7.4), 150 mM NaCl, 6.4 mM KCl, 2 mM $MgCl_2$, 0.005% Surfactant P2. Antibodies were injected at a flow rate of 10 μl/min at 1 μM IgG or 500 nM Fab in running buffer, respectively. The bound antibodies were removed by injecting a pulse of 100 mM glycine/HCl (pH 2.8). The analysis was carried out on the BIAlite upgrade system, employing BIA evaluation software version 3.1 (BIACORE).

Immunoprecipitation—For co-immunoprecipitation, HeLa cells were transfected with an expression plasmid (pCAGGSM2-IRES-GFP) coding for *BIP*-His_6 using Lipofectamine® (Invitrogen) according to the manufacturer's instructions. Two days after transfection, cells were washed twice with PBS (Gibco) and lysed in ice-cold CellLytic-M lysis buffer with protease inhibitor mixture (Sigma) (37). After centrifugation at 16,000 × *g* and 4 °C for 10 min, supernatant was collected and precleared for 1 h with protein G beads (GE Healthcare). Subsequently, aliquots were incubated with two negative control antibodies (non-immune murine immunoglobulins and anti-GFP) or anti-hexahistidine and anti-BiP antibodies at 4 °C overnight, respectively. Precipitation of immune complexes was performed by the addition of protein G beads for 8 h at 4 °C. The beads were washed three times with Nonidet P-40 buffer (150 mM NaCl, 50 mM Tris-HCl, pH 7.4, and 1% Nonidet-P40) and subjected to SDS-PAGE and Western blotting. For detection, Sec61α and BiP rabbit polyclonal antibodies were used. The primary antibodies were visualized using secondary POD-coupled anti-rabbit antibody (Sigma) and ECL.

For immunoprecipitation, canine pancreatic rough microsomes (RM) were stripped of ribosomes with puromycin and high salt, yielding puromycin and high salt treated RM (PKRM), and solubilized in 50 mM HEPES/KOH, pH 7.8, 500 mM KAc, 15% glycerol, 2.5% digitonin for 10 min on ice as described (25). Supernatant was collected after centrifugation at 16,000 × *g* and 4 °C for 10 min. Antibodies were coupled according to the manufacturer's protocol to Dynabeads-Protein A (DYNAL BIOTECH), and the loaded beads were incubated with the solubilized PKRM overnight at 4 °C with slow shaking. After removing the supernatant, the beads were washed three times with 1 ml of Nonidet P-40 buffer (150 mM NaCl, 50 mM Tris-HCl, pH 7.4, and 1% Nonidet-P40) and, subsequently, incubated with 100 mM glycine/HCl (pH 2.8) for 30 min at room temperature. Supernatant was collected and neutralized, SDS-sample buffer was added, and the sample was incubated for 10 min at 56 °C. The samples were analyzed by SDS-PAGE and Western blotting. For Sec61 detection, the Sec61 α-subunit-specific rabbit polyclonal antibody was used as well as a secondary POD-coupled anti-rabbit antibody (Sigma) and ECL™, visualized with a Fusion SL (peqlab) luminescence imaging system.

Single Channel Recordings—Vesicles for planar bilayer experiments were prepared by mixing (3:2, v/v) the Sec61-containing vesicles with preformed liposomes (egg L-α-phosphatidylcholine, 10 mg/ml) in 50 mM KCl and 10 mM Mops/Tris (pH 7.0) (9). Mega-9 (nonanoyl-*N*-methylglucamide) was added to a final concentration of 80 mM. After mixing, the sample was dialyzed for 4 h at room temperature and then overnight at 4 °C against a buffer containing 50 mM KCl and 10 mM Mops/Tris (pH 7.0). Aliquots (10 μl, typically 10 mg/ml protein, lipid/protein 2:1 (w/w)) of the proteoliposomes derived from rough microsome vesicles were incubated with 200 μM puromycin and 250–500 mM KCl for 15–30 min on ice. Planar lipid bilayers were produced by the painting technique described previously

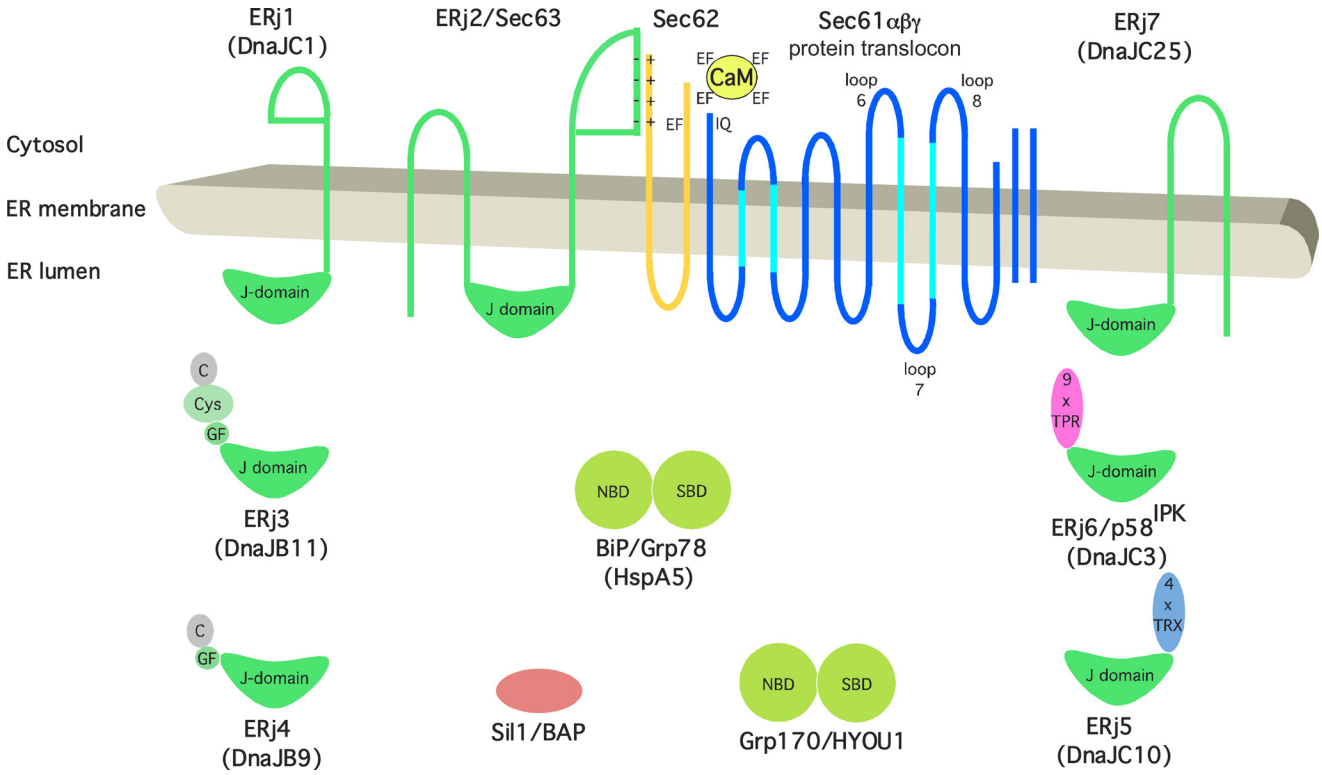

FIGURE 1. **Topology and domain organization of Sec61 complex, Sec62, BiP and its Hsp40-type co-chaperones and nucleotide exchange factors in the ER of human cells.** Protein names, synonyms, and systematic chaperone names (in parentheses) are indicated. *C*, carboxyl-terminal or substrate binding domain; *Cys*, cysteine-repeat or zinc finger-like domain; *EF*, EF-hand motif; *GF*, glycine/phenylalanine-rich domain; *IQ*, IQ motif; *NBD*, nucleotide binding domain; *SBD*, substrate binding domain; *TPR*, tetratricopeptide repeat; *TRX*, thioredoxin domain.

(38). An osmotic gradient was used for vesicle fusion. Membrane potentials refer to the trans compartment. Data recording and analysis were performed as described previously (9). Voltage ramps were conducted at a rate of 6.6 mV/s.

Cell Migration Analysis—Migration was tested with the BD Falcon FluoroBlok system (BD Biosciences) in 24-well inserts (22). A total of 2.5×10^4 cells treated with control siRNA or siRNAs against *ERJ3* and *ERj6*, respectively, for 48 h were loaded into this system in DMEM containing 1.0% FBS. The inserts were placed in DMEM with 10% FBS as an attractant. After 48 h, the cells were fixed with methanol and stained with DAPI, and migrating cells were analyzed at room temperature on the backside of the membrane by fluorescence microscopy on a TE2000-S inverted microscope (Nikon). The microscope was equipped with a Plan Fluor lens with 10× magnification and 0.3 numerical aperture (Nikon) and a Digital Sight DS-5Mc camera (Nikon). Migrated cells of at least three individual images were automatically counted using NIS-Elements AR Software (Nikon).

Peptide Spot Array for Antibody Characterization—Peptides (12 amino acid residues with an overlap of 10 residues) covering the whole length of Sec61α were synthesized on acid-hardened cellulose membranes, derivatized with a polyethylene glycol spacer, as described (39). Membranes were equilibrated in 150 mM NaCl, 50 mM Tris/HCl (pH 7.5) for 30 min at room temperature. The diluted antibody (1:1,000) in PBS (5% milk powder) was added, and the membrane was incubated at 4 °C overnight. Thereafter, the membrane was washed twice with PBS buffer for 10 min, incubated with POD-coupled anti-rabbit antibody (Sigma), washed twice with PBS, incubated with ECL, and analyzed using a LumiImager F1 workstation (Roche Applied Science). Stripping of the bound antibodies was performed by incubating the membranes with 100 mM glycine/HCl (pH 2.8) for 30 min at room temperature and repeated washing with PBS.

Results

Silencing of ERJ3 and ERJ6 Stimulates ER Calcium Leakage in Intact Cells—Based on the previous *in vitro* and cellular level experiments, we expected Hsp40-type co-chaperones of BiP to contribute to the limiting of Sec61-mediated Ca^{2+} efflux from the ER (16, 17). Seven such co-chaperones are currently known in the mammalian ER and were termed ERdj or ERj proteins 1–7 (40, 41) (Fig. 1 and Table 2). Because the ER membrane protein Sec63 acts as BiP co-chaperone in facilitating protein transport into the mammalian ER (33), we first investigated whether silencing the *SEC63* gene in HeLa cells with an established siRNA enhanced Ca^{2+} efflux from the ER. The same siRNA was previously shown to result in precursor polypeptide-specific inhibition of protein transport into the ER of HeLa cells (33). Using the Ca^{2+} dye Fura-2 in the absence of extracellular Ca^{2+} allows visualization of Ca^{2+} leakage from the ER, indicated by the increased cytosolic calcium concentration in intact cells in response to the irreversible SERCA inhibitor thapsigargin. In Ca^{2+} imaging experiments, HeLa cells were treated with *SEC63* siRNA for 96 h, and subsequently, Ca^{2+} leakage was unmasked by application of thapsigargin in the presence of extracellular EGTA. Cells treated with a non-tar-

TABLE 2

Properties of BiP and its co-chaperones and nucleotide exchange factors

The concentration of ERj6 was determined for a suspension of canine pancreatic microsomes as described previously for the listed proteins (27, 28). The binding constants of ERj4, ERj5, and ERj7 for hamster BiP were taken from previous publications (27, 28, 39). We note that our other previously published binding constants of ERj1, -2, and -3 as well as full-length ERj5 referred to murine BiP and showed significant differences only with respect to ERj3 (K_D = 3.6). Similar to human patients with MSS, mice homozygous with respect to the so-called woozy mutation in the *Sil1* gene develop ataxia, due to Purkinje cell loss in the cerebellum, and myopathy (72). HUS, hemolytic uremic syndrome; MSS, Marinesco-Sjögren syndrome; PLD, polycystic liver disease.

Protein	UPR-controlled	Recombinant protein (amino acid residues)	Binding constants for BiP in the presence of ATP			Molar ratio to BiP in ER lumen	Associated diseases in	
			k_{on}	k_{off}	K_D		Humans	Mice
			$M^{-1}s^{-1}$	s^{-1}	μM			
BiP	+	BiP-hexahis (20–655)	not determined			1	HUS	
ERj1	−	GST-J1 domain (44–140)	4.2×10^4	1.9×10^{-3}	0.17	0.07		
ERj2	−	GST-J2 domain (91–189)	1.2×10^3	3.4×10^{-3}	2.91	0.40	PLD	PLD
ERj3	+	GST-ERj3 (18–358)	4.1×10^3	2.2×10^{-3}	0.57	0.06		
ERj4	+++	GST-ERj4 (24–222)	0.5×10^3	3.2×10^{-3}	6.07	Not detectable		Diabetes
ERj5	+	GST-J5 domain (26–123)	2.8×10^3	1.7×10^{-3}	0.59	0.40		
ERj6	+	GST-ERj6 (32–504)	3.9×10^2	1.9×10^{-3}	5.00	0.03	Diabetes	Diabetes
ERj7	+	GST-J7 domain (39–149)	5.1×10^3	5.7×10^{-3}	1.13	0.46		
Grp170	+		Not determined			0.12		
Sil1	−	GST (39–461)	Not detectable			0.001	MSS	"Woozy" phenotype

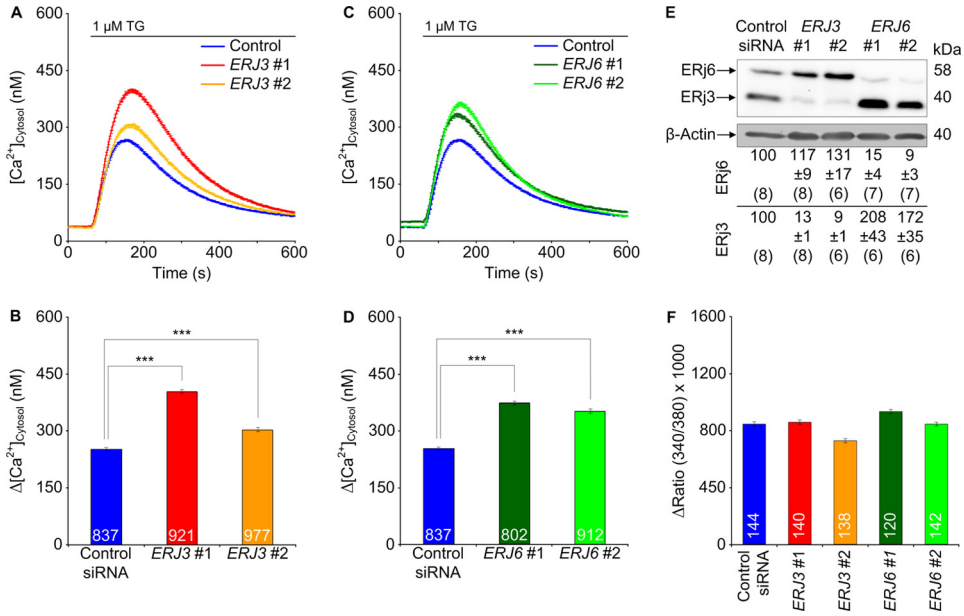

FIGURE 2. **Effect of depletion of the ER lumenal Hsp40s, ERj3 and ERj6, on Ca^{2+} leakage from the ER in HeLa cells.** *A* and *C*, HeLa cells were treated with the indicated siRNAs for 96 h and loaded with the calcium indicator Fura-2 AM as described under "Experimental Procedures." Then live cell Ca^{2+} imaging was carried out according to our established procedure (13, 14, 16). Ca^{2+} release was unmasked by applying thapsigargin (1 μM) in the presence of external EGTA. Average values are given, and *error bars* represent S.E. *B* and *D*, statistical analysis of the changes in the cytosolic Ca^{2+} concentration after the addition of thapsigargin in the experiments presented in *A* and *C*. *Error bars*, S.E. *p* values of <0.001 were defined as significant by unpaired *t* tests and are indicated by *three asterisks*. The numbers of cells that were analyzed are indicated. Data were collected in six independent experiments with culture duplicates for each condition. In these experiments, the averaged numbers of silencing siRNA-treated cells corresponded to 78 ± 9, 83 ± 6, 79 ± 12, and 89 ± 10%, respectively, as compared with control siRNA-treated cells. *E*, silencing was evaluated by Western blots. Averaged relative protein contents are given with S.E. as a percentage of control siRNA-treated cells and as normalized to β-actin (*n* is given in *parenthesis*). Only the areas of interest from single gels are shown. *F*, HeLa cells were treated and analyzed as described for *A–D*, except that ionomycin (5 μM) was used instead of thapsigargin in order to measure total cellular calcium according to our established procedure (16). Data were accumulated in a single experiment with culture duplicates for each condition. Because the calibration did not cover the high concentrations in the cytosolic Ca^{2+} concentration after the addition of ionomycin, we refrained from converting these ratios to cytosolic Ca^{2+} concentrations.

geting siRNA were subjected to the same procedure and served as negative control. In comparison with the control siRNA, the *SEC63* siRNA had no effect at all on the thapsigargin-induced Ca^{2+} efflux, with a silencing rate of about 80% (data not shown). This suggests that Sec63 does not contribute to the limiting of Ca^{2+} leakage from the ER in human cells. Because the Sec63-related ER membrane-resident Hsp40, ERj1, was previously found to be unable to support BiP in Sec61 channel closure (14), we asked in the next experiment whether simultaneous depletion of all three known ER membrane-resident Hsp40s with a lumenal J-domain (ERj1, ERj2/Sec63, and ERj7) would enhance Ca^{2+} efflux from the ER (25, 28, 42, 43). Still, no effect was observed, although the silencing rate was above 75% (data not shown). Thus, the membrane-resident BiP co-chaperones apparently do not contribute to the limiting of Ca^{2+} leakage from the ER in human cells.

Next, we investigated whether knockdown of the ER lumenal Hsp40s (ERj3, ERj4, ERj5, and ERj6) enhances Ca^{2+} efflux from the ER in HeLa cells (44–49). Because ERj3 and ERj6 were found to associate with the Sec61 complex (50, 51), we first treated HeLa cells with two different *ERJ3* or *ERJ6* siRNAs and carried out Ca^{2+} imaging as described above. In contrast to the control siRNA, the *ERJ3* and *ERJ6* siRNAs significantly enhanced the thapsigargin-induced Ca^{2+} efflux (Fig. 2, *A–D*).

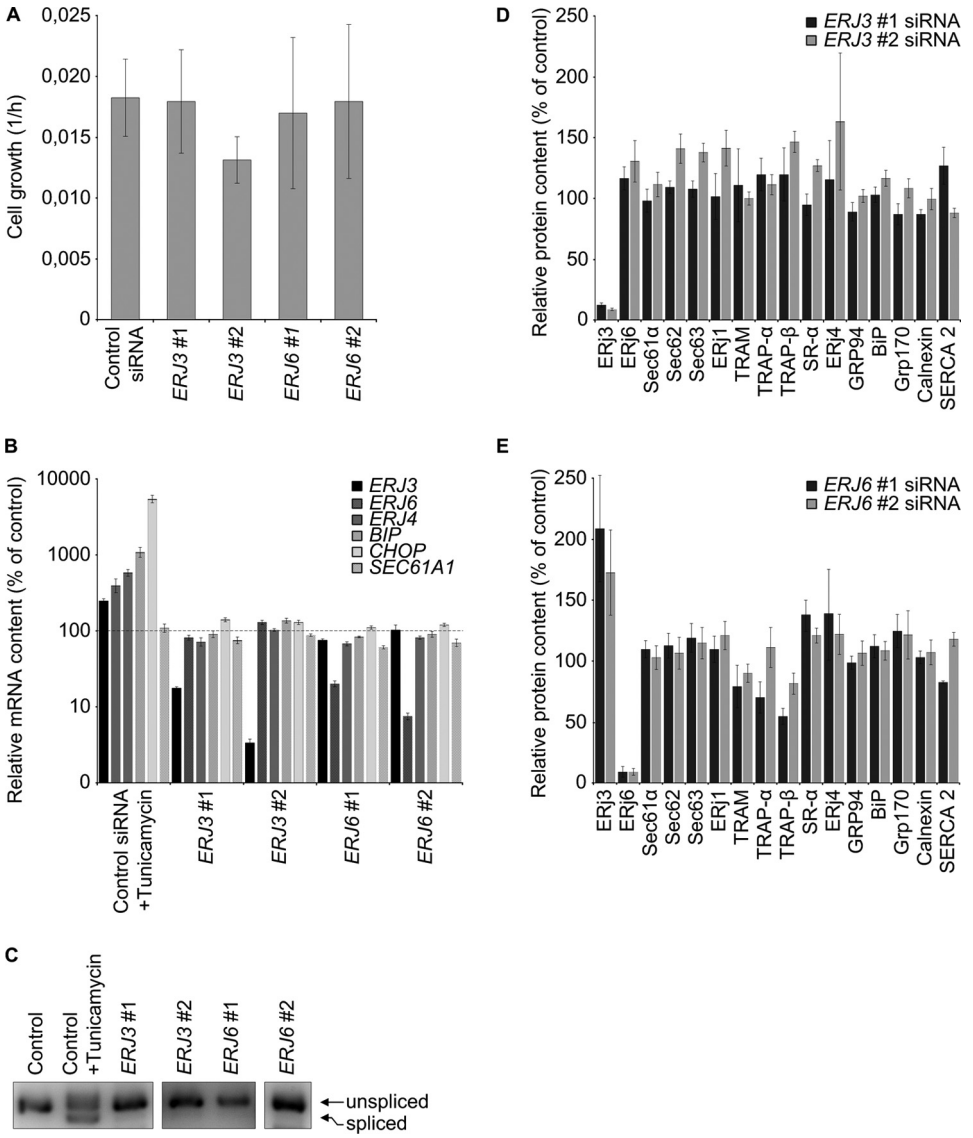

FIGURE 3. **Effect of *ERJ3* and *ERJ6* gene silencing on cell proliferation and the content of selected mRNAs and proteins.** *A*, HeLa cells were treated with the indicated siRNAs for 48 h and seeded in E-plates. Proliferation was recorded in real time for 48 h. Growth rates were measured in three independent experiments in triplicate and are given with S.E. (*error bars*) as slope of the curves for the second 48 h. Silencing was evaluated by Western blots (data not shown). *B–E*, HeLa cells were treated with the indicated siRNAs for 96 h as in Fig. 2, and their content of selected mRNAs and proteins, respectively, was evaluated by quantitative real-time PCR (*B*), agarose gel electrophoresis (*C*), or Western blots (*D* and *E*). *B* and *C*, as positive control for UPR activation, control siRNA-treated cells were treated with tunicamycin for 5 h at 2 μg/ml. *B*, averaged relative mRNA contents from four independent experiments are given with S.E. as a percentage of control siRNA-treated cells and as normalized to *ACTB*. The 100% values are indicated by a *dashed line*. *C*, *XBP1* was amplified in the same cDNA as in *B* with appropriate primers and subjected to gel electrophoresis and imaging. Only the area of interest from a single 3% agarose gel is shown. *Lanes 4* and *5* represent a longer exposure as compared with the other lanes. *D* and *E*, for Western blots, averaged relative protein contents are given with S.E. as a percentage of control siRNA-treated cells and as normalized to β-actin.

In these experiments, the silencing rate was above 80% (Fig. 2*E*). Thus, the ER lumenal BiP co-chaperones, ERj3 and ERj6, contribute to the limiting of Ca^{2+} leakage from the ER in human cells. We suggest that in the case of ERj3 knockdown with two different siRNAs, which resulted in similar silencing efficiencies but quantitatively different effects on Ca^{2+} efflux from the ER, the differences may have been due to different silencing rates.

Control experiments, using ionomycin instead of thapsigargin, confirmed that the enhanced ER Ca^{2+} leakage in ERj3- or ERj6-depleted cells was not due to elevated cellular Ca^{2+} concentration in these cells (Fig. 2*F*) and gross alterations in cell or ER morphology (three-dimensional SIM data not shown). Additional control experiments demonstrated the integrity of the depleted cells in the course of the experiments; ERj3 and ERj6 depletion (i) hardly affected cell growth (Fig. 3*A* and legend to Fig. 2), (ii) did not affect ER import of three model precursor polypeptides (preprolactin, preproapelin, and prestatherin) (data not shown), (iii) did not lead to activation of the unfolded protein response (*i.e. BIP*, *ERJ4*, and *CHOP* mRNAs were not overproduced, and *XBP1* mRNA was not spliced) (Fig. 3, *B* and *C*), and (iv) did not result in global effects on the ER proteome (Fig. 3, *D* and *E*). However, *ERJ6* silencing reproducibly led to an increased ERj3 protein content (Figs. 2*E* and 3*E*). This raised the question of why increased ERj3 levels did not compensate for the decreased ERj6 levels in limiting Ca^{2+} leak-

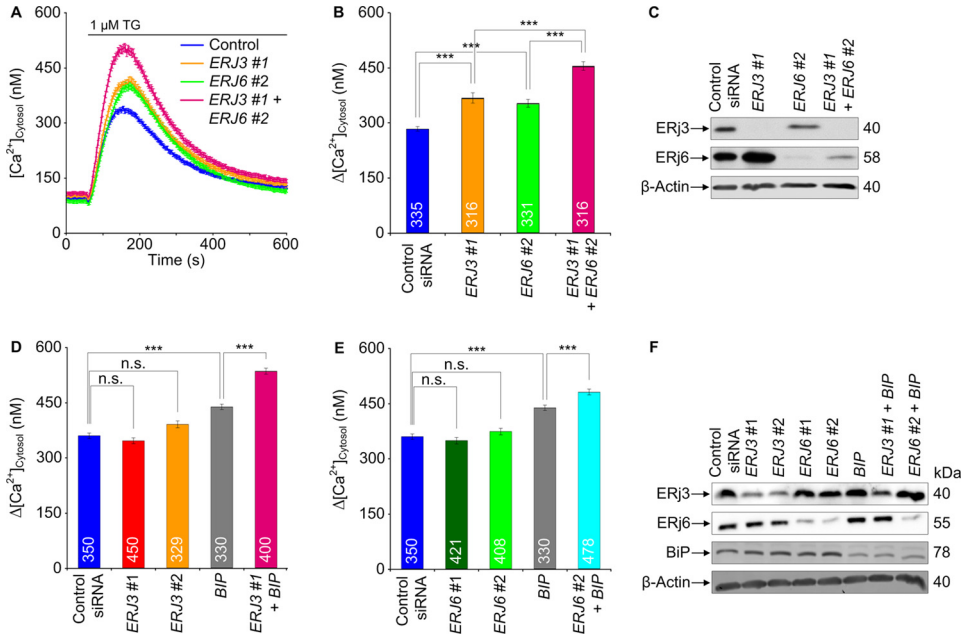

FIGURE 4. **Effect of simultaneous depletion of ER lumenal Hsp40s, ERj3 and ERj6, and BiP on Ca^{2+} leakage from the ER in HeLa cells.** *A*, HeLa cells were treated with the indicated combinations of siRNAs for 96 h and analyzed as described in the legend to Fig. 2. Average values are given, and *error bars* represent S.E. *B*, *D*, and *E*, statistical analysis of the changes in the cytosolic Ca^{2+} concentration after the addition of thapsigargin. *Error bars*, S.E. *p* values of <0.001 were defined as significant by unpaired *t* tests and are indicated by *three asterisks*. The numbers of cells that were analyzed are indicated. Data were collected in two (*B*) or three (*D* and *E*) independent experiments with culture duplicates for each condition. *C* and *F*, silencing was evaluated by Western blots. Only the areas of interest from single gels are shown.

age from the ER. We propose that the two co-chaperones may act in a complex and will pursue this idea in future experiments.

We wondered whether simultaneous depletion of ERj3 and ERj6 has a more pronounced effect on Ca^{2+} efflux from the ER, as compared with the separate knockdowns, and found this to be the case (Fig. 4, *A–C*). We not only analyzed Ca^{2+} efflux from the ER in response to ERj3 plus ERj6 knockdown indirectly (*i.e.* as increased Ca^{2+} concentration in the cytosol) but also did so directly by simultaneous monitoring of ER lumenal Ca^{2+} concentration. HeLa cells were stably transfected with a plasmid that codes for the ER-targeted Ca^{2+} sensor protein D1ER. ERj3 and ERj6 were simultaneously depleted for 96 h, and the cells were loaded with Fura-2 as before. Subsequently, Ca^{2+} efflux was unmasked by thapsigargin, and the Ca^{2+} concentrations in cytosol and ER lumen were monitored by Fura-2 and FRET imaging, respectively (Fig. 5). In contrast to the control siRNA, the combination of *ERJ3* and *ERJ6* siRNAs simultaneously enhanced the thapsigargin-induced Ca^{2+} decrease in the ER lumen and increase in the cytosol. Thus, there was a correlation between increasing Ca^{2+} concentration in the cytosol and decreasing Ca^{2+} concentration in the ER lumen in response to ERj3 plus ERj6 depletion (*i.e.* Ca^{2+} was indeed leaking from the ER into the cytosol after ERj3 and ERj6 depletion). A similar additive effect as after simultaneous depletion of ERj3 and ERj6 was observed when *ERJ3* or *ERJ6* siRNA was combined with *BIP* siRNA (Fig. 4, *D–F*). We note that in these latter experiments, silencing was carried out for only 48 h, which explains why the separate Hsp40 knockdowns had hardly any effect. These results were consistent with the notion that both ERj3 and ERj6 contribute to BiP-mediated Sec61 channel closure in human cells.

To confirm these conclusions, we attempted complementation by the *ERJ3* cDNA lacking the *ERJ3*-UTR in the presence of the *ERJ3*-UTR siRNA and observed rescue of the *ERJ3* silencing phenotype in the form of restoration of the basal ER Ca^{2+} efflux seen in control cells (Fig. 6, *A–C*). Of note, transfection with a negative control plasmid had no effect.

To address the question of whether the observed effects of ERj3 and ERj6 on cellular Ca^{2+} homeostasis are specific or a general phenomenon of ER lumenal BiP co-chaperones, we investigated whether silencing the *ERJ5* gene in HeLa cells with validated siRNAs enhanced Ca^{2+} efflux from the ER. In contrast to the ERj3 and ERj6 depletion, the depletion of ERj5 did not have a stimulatory effect on Ca^{2+} efflux (Fig. 6, *D–F*) under conditions of an average silencing rate of 80%. Similar results were obtained with two established siRNAs against *ERJ5* (data not shown), which caused an ER protein export defect (52). Thus, the observed co-chaperoning effect is specific to ERj3 and ERj6. We note that ERj4 was omitted from this analysis because it is typically detectable only after induction of the unfolded protein response (40, 41, 45).

Next, we asked whether the effects of ERj3 and ERj6 on ER Ca^{2+} leakage could be linked to the Ca^{2+}-permeable Sec61 complex. To address this question, we treated HeLa cells for 96 h with siRNA directed against *ERJ3* or *ERJ6* plus either *SEC61A1* siRNA or a negative control siRNA. Ca^{2+} imaging experiments showed that additional silencing of *SEC61A1*, but not the control silencing, in the presence of *ERJ3* or *ERJ6* siRNA prevented the *ERJ* silencing-induced Ca^{2+} efflux (Fig. 7, *A–D*). According to Western blot analysis, the silencing efficiency of all three siRNAs was above 80% (Fig. 7*E*). Thus, ERj3 and ERj6 contribute to reducing Ca^{2+} leakage from the ER at the level of

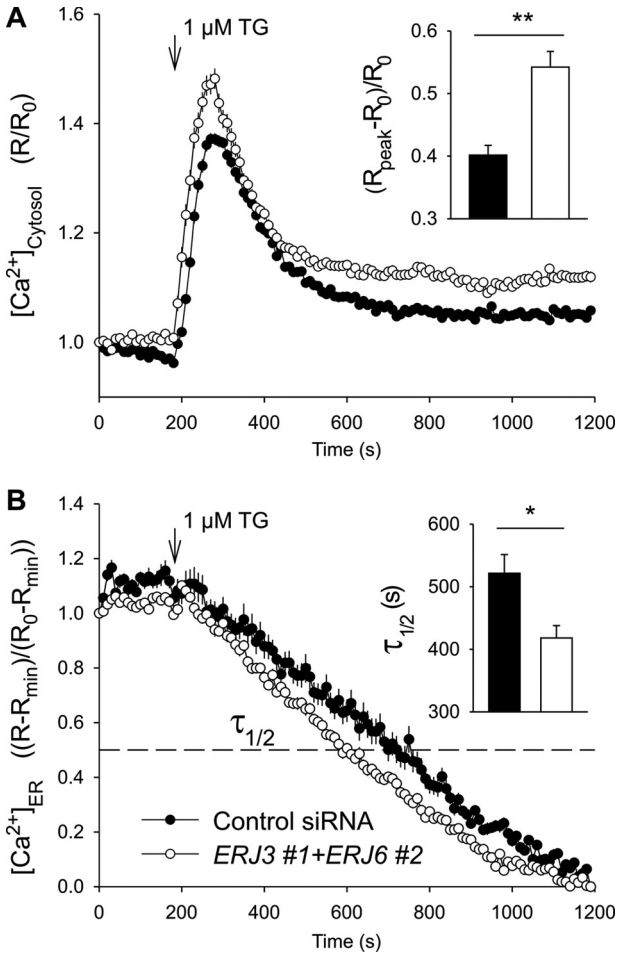

FIGURE 5. **Effect of simultaneous depletion of ERj3 and ERj6 on ER lumenal Ca^{2+} in HeLa cells.** The FRET-based sensor D1ER was stably expressed in HeLa-D1ER cells and used to image the ER lumenal Ca^{2+} ($[Ca^{2+}]_{ER}$). The gene silencing was carried out with the indicated siRNAs for 96 h. Just before imaging, cells were loaded with Fura-2 AM to image the cytosolic Ca^{2+} ($[Ca^{2+}]_{cytosol}$) and incubated in a Ca^{2+}-free solution containing EGTA. The Ca^{2+} leakage was unmasked with thapsigargin (1 μM). The time courses of $[Ca^{2+}]_{cytosol}$ (*A*) and $[Ca^{2+}]_{ER}$ (*B*) were obtained in the same cells. $n = 38$ (control siRNA) and 22 (*ERJ3* + *ERJ6* siRNA). To evaluate the effects of gene silencing, we calculate the $\Delta[Ca^{2+}]_{cytosol}$ as $(R_{peak} - R_0)/R_0$, where R represents the ratio F_{340}/F_{380} of Fura-2 signals (*A*, *inset*). The time to 50% decay ($\tau_{1/2}$) of $[Ca^{2+}]_{ER}$ was measured in individual cells (*B*, *inset*).

the Sec61 complex. We note that *SEC61A1* silencing led to depletion of ERj3 and ERj6 in these experiments, which must be due to their Sec61-dependent ER import.

In the next experiments, we characterized the interaction between BiP and its Hsp40-type co-chaperones by surface plasmon resonance spectroscopy. GST fusion proteins of ER-resident Hsp40s, ERj3 and ERj6, were purified and functionally characterized by surface plasmon resonance spectroscopy. As expected, both Hsp40s were able to productively interact with BiP, albeit with different affinities (Fig. 8 and Table 2). The affinity of ERj3 for hamster BiP was calculated, based on Fig. 8, as 0.57 μM (Table 2). The affinity of ERj6 had not previously been determined and was calculated as 5 μM (Table 2).

BiP and Antibodies Directed against the BiP Binding Site Can Bind to the Sec61α Subunit That Is Present in the Native Sec61 Complex—Our previous analysis demonstrated the interaction of BiP with loop 7 of Sec61α at the peptide level and *in silico* (16). Here, we addressed the question of whether loop 7 of Sec61α is available to BiP binding in the native Sec61 complex, using various experimental strategies. First, we asked whether Sec61α can be co-immunoprecipitated together with BiP from HeLa cell extract under established immunoprecipitation conditions (37). HeLa cells were transfected with a plasmid, coding for BiP with a hexahistidine tag. Two days after transfection, the cells were lysed and, after a preclearing step with protein G beads, aliquots were incubated with two negative control antibodies (non-immune murine immunoglobulins or anti-GFP) and anti-hexahistidine and anti-BiP antibodies, respectively. Subsequently, the immunocomplexes were harvested with protein G beads and, after three washing steps, subjected to SDS-PAGE and Western blotting. The nitrocellulose membranes were probed with anti-BiP and anti-Sec61α antibodies and secondary peroxidase-coupled antibodies. The chemiluminescent signals were detected (Fig. 9*A*). Both anti-hexahistidine and anti-BiP antibodies precipitated BiP and co-immunoprecipitated Sec61α, whereas the negative control antibodies failed to do so. Thus, BiP and Sec61 complex are associated with each other under normal growth conditions, as had been observed previously (53).

Next we asked whether antibodies and Fab fragments directed against the dityrosine-containing motif within loop 7, which was characterized as a BiP interaction site (16), can access their epitope within native Sec61 complex. An antipeptide antibody was raised against the oligopeptide GGLCYYLSPPESC, corresponding to amino acid residues 339–350 of human Sec61α plus a carboxyl-terminal cysteine residue, and affinity-purified. The purified antibodies were characterized as monospecific and of high affinity by Western blot, peptide library, and surface plasmon resonance experiments (Fig. 10, *A*, *B*, and *D*). These antibodies were able to immunoprecipitate native Sec61 complex from canine pancreatic microsomal extracts (Fig. 9*B*), albeit less efficiently as compared with Sec61β antibodies (25). Thus, the tyrosine 344-containing motif within loop 7 of Sec61α is available to antibody binding in the native Sec61 complex.

Because we previously have observed Sec61 channel activity and its inhibition by BiP in single channel recordings from reconstituted canine pancreatic microsomes (9), we also addressed the question of whether anti-loop 7-Fabs can access their epitope in the membrane-integrated Sec61 complex and whether or not their binding affects channel gating. Fab fragments were purified and characterized by surface plasmon resonance spectroscopy (Fig. 10, *C* and *D*). In contrast to an affinity-purified anti-Sec61β antibody, binding of the anti-loop 7-Fabs to the Sec61 complex induced channel closure (Fig. 9, *C–F*); specifically, the slopes of the current voltage relations in *C* and *D* are nearly identical (slope = 1.29 nS in *C* and 1.22 nS in *D*). The two single current voltage sweep measurements were from the same bilayer containing two channels, which did not change their open state during the voltage sweep between $V_m = -50$ and $V_m = +50$ mV. Closure of Sec61 channels was mainly but not exclusively observed at $|V_m| \geq 50$ mV. The conductance histograms in Fig. 9, *E* and *F*, are averages from three different single channel recordings during a 1-min voltage gate of $V_m = 40$ mV.

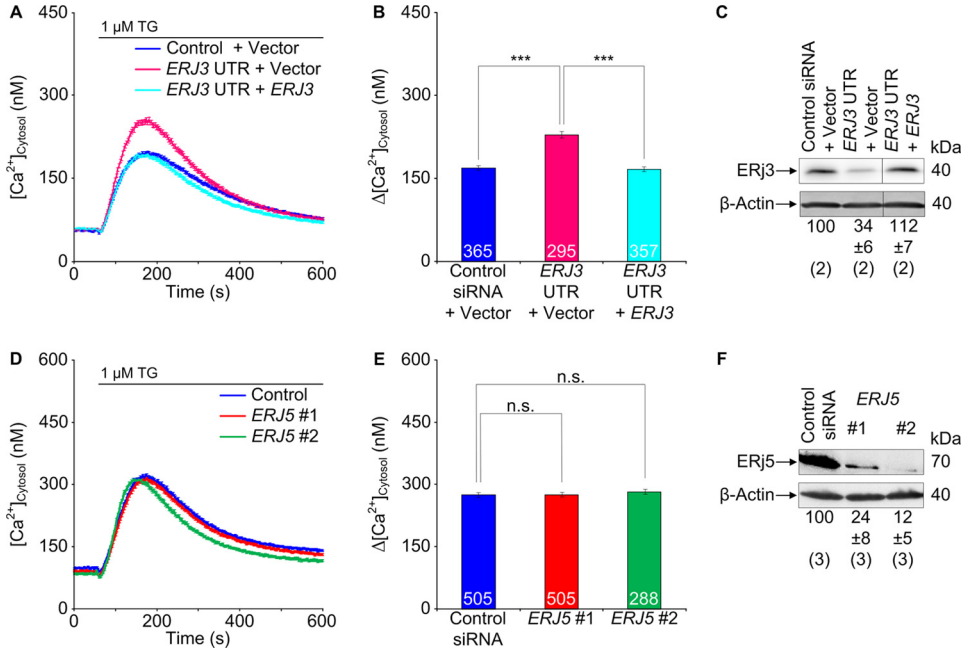

FIGURE 6. **Effects of *ERJ3* expression and ERj5 depletion, respectively, on Ca^{2+} leakage from the ER in HeLa cells.** *A*, HeLa cells were treated with the indicated siRNAs and plasmids for 96 h and analyzed as described in the legend to Fig. 2. Average values are given, and *error bars* represent S.E. *D*, HeLa cells were treated with the indicated siRNAs (10 nM) for 72 h and analyzed as described in the legend to Fig. 2. Average values are given, and *error bars* represent S.E. *B* and *E*, statistical analysis of the changes in the cytosolic Ca^{2+} concentration after the addition of thapsigargin in the experiments presented in *A* and *D*, respectively. *Error bars*, S.E. *p* values of <0.001 were defined as significant by unpaired *t* tests and are indicated by *three asterisks*. The numbers of cells that were analyzed are indicated. *B*, data were collected in two independent experiments with culture triplicates for each condition. *E*, data were collected in five independent experiments with culture duplicates for each condition. In these experiments, the averaged numbers of silencing siRNA-treated cells corresponded to 94 ± 23 and 96 ± 15%, respectively, as compared with control siRNA-treated cells. *C* and *F*, expression and silencing, respectively, were evaluated by Western blots. Averaged relative protein contents are given with S.E. at a percentage of control siRNA-treated cells and as normalized to β-actin (*n* is given in *parenthesis*). Only the areas of interest from single gels are shown. *n.s.*, not significant.

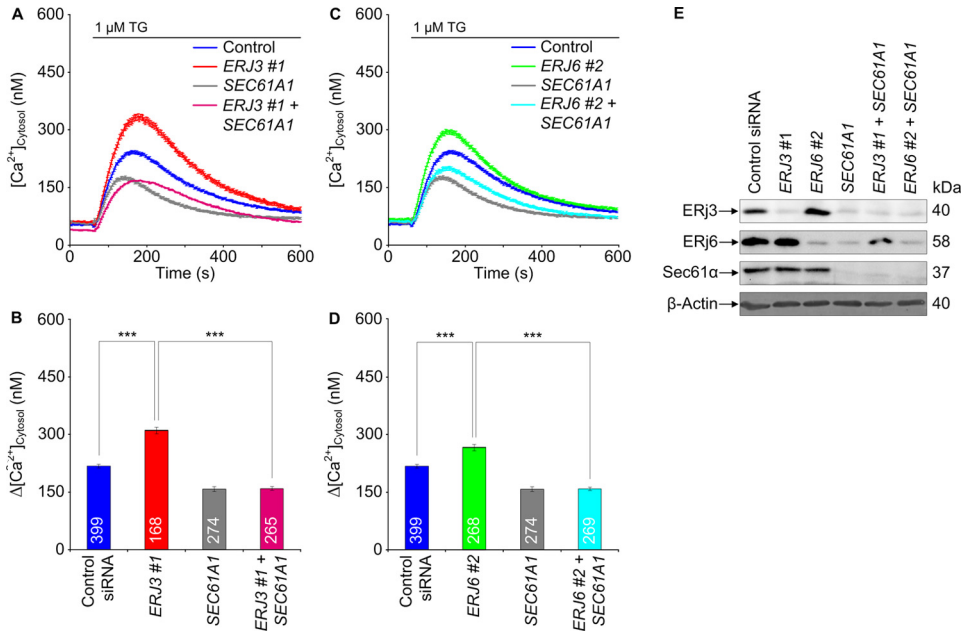

FIGURE 7. **Effect of simultaneous depletion of ER lumenal Hsp40s, ERj3 and ERj6, and Sec61 complex on Ca^{2+} leakage from the ER in HeLa cells.** *A* and *C*, HeLa cells were treated with the indicated siRNAs for 96 h and loaded with the calcium indicator Fura-2 AM as described under "Experimental Procedures." Then live cell Ca^{2+} imaging was carried out. Ca^{2+} release was unmasked by applying thapsigargin in the absence of external Ca^{2+}. Average values are given, and *error bars* represent S.E. *B* and *D*, statistical analysis of the changes in the cytosolic Ca^{2+} concentration after the addition of thapsigargin in the experiments presented in *A* and *C*. *Error bars*, S.E. *p* values of <0.001 were defined as significant by unpaired *t* tests and are indicated by *three asterisks*. The numbers of cells that were analyzed are indicated. Data were collected in two independent experiments with culture duplicates for each condition. *E*, silencing was evaluated by Western blots. Only the areas of interest from single gels are shown.

The data indicate that the anti-loop 7 Fab shifted the population of the Sec61 open channel states toward the closed state. Thus, these results confirmed that loop 7 is accessible to soluble proteins in native Sec61 complexes and suggested that binding of even an artificial ligand to loop 7 is sufficient to induce Sec61 gating. We note that Fabs against the cyto-

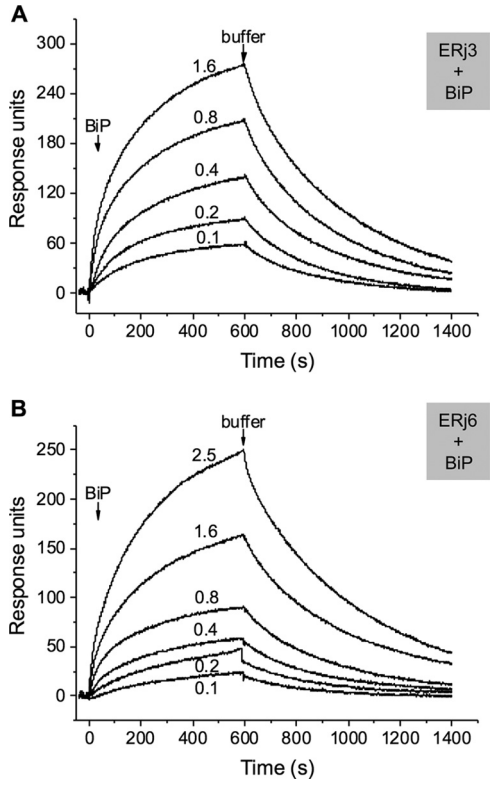

FIGURE 8. **Interaction of ER-resident Hsp40s with BiP.** The GST hybrid proteins of ERj3 (*A*) and ERj 6 (*B*), respectively, were immobilized in the measuring cell; GST was bound in the reference cell. BiP binding was analyzed in a BIAlite upgrade system at the indicated analyte concentrations (in μM) in comparison with the reference cell, according to our established procedure (25–28).

solic ribosome binding site in *Thermus thermophilus* SecYE were able to induce partial channel opening in this ortholog of the Sec61 complex (54).

ERJ3 and ERJ6 Silencing Phenocopies the Effects of SEC62 Silencing and Calmodulin Inactivation in Inhibition of Migration of Human Cells—We sought to independently, albeit indirectly, confirm the notion that depletion of ERj3 or ERj6 from human cells leads to Ca^{2+} leakage from the ER and, therefore, a rise in the cytosolic Ca^{2+} concentration. In previous experiments, we observed that Ca^{2+} leakage from the ER can be induced in various human tumor cells by depletion of the ER membrane protein Sec62 as well as by inhibition of CaM by CaM antagonists, such as ophiobolin A and trifluoperazin (18, 23). Both treatments resulted in a rise in the cytosolic Ca^{2+} concentration and a reduction of the cells' ability to migrate in an established transwell migration assay (18, 23, 55). Therefore, we tested whether silencing of the *ERJ3* or *ERJ6* gene has a similar effect and found this to be the case; cell migration decreased to 22 ± 4%, 12 ± 3%, 5 ± 1%, and 14 ± 2% after knockdown of ERj3 and ERj6, respectively, with two siRNAs each as compared with control siRNA-treated cells (data not shown). We note that silencing of both genes hardly affected cell growth (Fig. 3*A*) and that silencing of the *ERJ1* or *SEC63* gene did not have any effect on cell migration (23). Thus, the independent approach confirmed our interpretation that ERj3 and ERj6 are involved in controlling Ca^{2+} leakage from the ER.

Discussion

BiP Co-chaperones ERj3 and ERj6 Support BiP-mediated Gating of the Sec61 Channel—Previous work from a number of laboratories characterized the ER membrane-resident Sec61 complex, which facilitates transport of presecretory proteins into the ER and insertion of plasma membrane proteins into the ER membrane (10, 11), as a major ER Ca^{2+} leak channel (12–16, 56–59). Furthermore, it was observed *in vitro* as well as in intact cells that the ER lumenal Hsp70-type molecular chaperone, BiP, is involved in limiting ER Ca^{2+} leakage at the level of the Sec61 complex (8, 9, 16, 17, 53, 60) (Fig. 1). Taking advantage of mutant BiP variants, such as BiPR197E or BiPR197H, which cannot productively interact with Hsp40-type co-chaperones, it was concluded that the action of BiP in Sec61 channel closure involves a Hsp40-type co-chaperone (16, 17, 61). Here, we observed that the ER lumenal Hsp40s, ERj3 (44, 62, 63) and ERj6 (48, 49), act as BiP co-chaperones in Sec61 channel closure and that the ER membrane-resident Hsp40s, ERj1, ERj2/Sec63, and ERj7, do not play a role. This finding is consistent with the previous reports that ERj3 and ERj6 are in association with the Sec61 complex (50, 51) and that loss of ERj6 function in mice and humans causes pancreatic β-cell failure and diabetes (20, 64), which was also observed with the murine Sec61αY344H mutation that destroys the BiP binding site (16, 19). We note that ERj2/Sec63 was previously shown to be involved in protein transport in a substrate-specific manner and that lack of this function can cause polycystic liver disease in humans and mice (31, 65, 66).

In the case of Sec63, physical association with Sec62 and Sec61 allows the co-chaperone Sec63 to recruit BiP to the Sec61 complex for protein translocation (Fig. 1), whereas for ERj3 and ERj6 the mechanism should be different. We suggest that the substrate binding domains of the two co-chaperones, which are the carboxyl-terminal domain and tetratricopeptide repeat, respectively, may facilitate recruitment of BiP to the ER lumenal loop 7 of Sec61α for channel closure (67). Because of the spatial constraints, it appears to be highly unlikely that the co-chaperones also bind to loop 7.

BiP/Sec61 Channel Interaction via ER Lumenal Loop 7 of Sec61α—Our previous work demonstrated the interaction of BiP with loop 7 of Sec61α at the level of synthetic peptides and *in silico* (16). Therefore, we suggested that BiP mediates Sec61 channel gating via loop 7 (Fig. 1). This view was supported by the observations that (i) replacement of tyrosine 344 by histidine in loop 7 leads to reduced BiP binding (16), (ii) BiP and Sec61 complex co-immunoprecipitate (53), (iii) replacement of Sec61α by Sec61αY344H results in increased Ca^{2+} leakage from the ER and the inability of BiP to suppress this in HeLa cells (16), and (iv) the homozygous Sec61αY344H mutation causes pancreatic β-cell death and diabetes in mice (19). Here, we reproduced the co-immunoprecipitation data (Fig. 9*A*) and demonstrated that antibodies against a tyrosine 344-containing peptide have access to their epitope in detergent-solubilized Sec61 complexes (Fig. 9*B*) and that Fabs thereof not only have access to their epitope in membrane-resident Sec61 complex but also mediate channel closure (Fig. 9, *E* and *F*). Therefore, the concept that BiP mediates Sec61 channel gating via loop 7

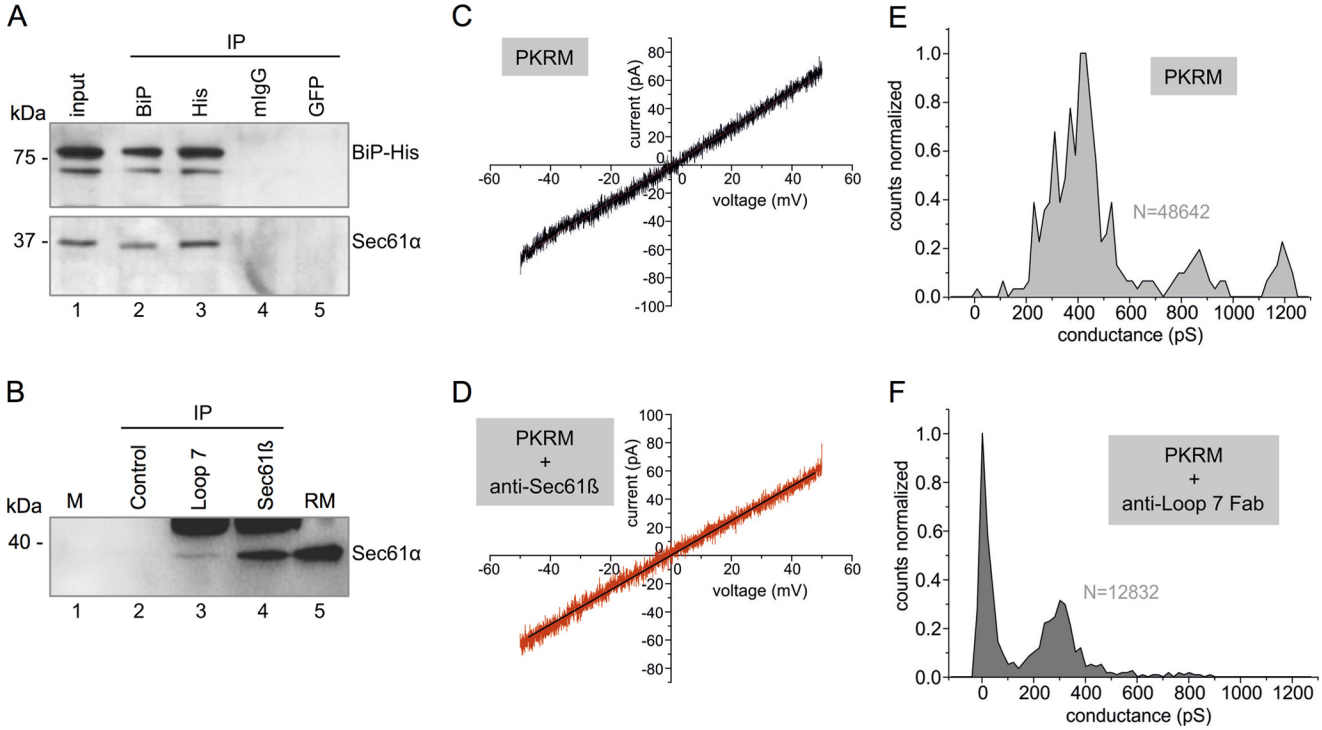

FIGURE 9. **Interaction of Sec61 complex with BiP and anti-loop 7 antibodies, respectively.** *A*, co-immunoprecipitation of BiP and Sec61 complex from BiP-His_6-containing HeLa cell extracts was carried out as described under "Experimental Procedures." The precipitates were analyzed for BiP and Sec61α, respectively. 40% of the HeLa cell extract that was used for the precipitation was analyzed in parallel (*lane 1*). Only the areas of interest from single gels are shown. *B*, pull-down of Sec61 complex from canine pancreatic microsomal extracts was carried out with anti-loop 7 antibodies as described under "Experimental Procedures." Affinity-purified anti-Sec61β antibodies served as positive control (*lane 4*). The precipitates were collected with Dynabeads. Dynabeads without antibody served as negative control (*lane 2*). Molecular mass marker (*M*) (*lane 1*) and rough canine pancreatic microsomes (rough microsomes; *RM*) (*lane 5*) were subjected to gel electrophoresis in parallel. All samples were analyzed for Sec61α. Only the areas of interest from single gels are shown. *C* and *D*, current voltage relationship from bilayers containing two active Sec61 channels in the absence or presence of affinity-purified anti-Sec61β at 2.5 μg/ml final concentration on both sides of the bilayer. *PKRM*, rough microsomes, which were treated with puromycin plus high salt, were used as the source of the Sec61 channels. *E* and *F*, conductance histograms from single channel recordings obtained from bilayers with single active Sec61 channels, average of $n = 3$ recordings at $V_m = +40$ mV in the absence of and after 30-min incubation with loop 7 Fabs (final concentration, 2 μg/ml).

interaction was further substantiated, and the idea that the energy of BiP binding to loop 7 is sufficient to mediate channel gating was experimentally confirmed.

Implications for the Link between ER Protein Misfolding, Ca^{2+} Homeostasis, and Apoptosis—As we have described previously, depletion of available BiP in cells by either *BIP* gene silencing or protein misfolding in the ER leads to Ca^{2+} leakage from the ER (16). It has been known for some time that protein misfolding in the ER initiates the unfolded protein response and, when the latter is unable to turn the tide, apoptosis, the underlying mechanisms of which are not fully understood (68, 69). Based on the observations that the *SEC61A1Y344H* mutation causes the unfolded protein response and apoptosis in a diabetes mouse model and that the same mutation destroys the BiP binding site and leads to increased ER Ca^{2+} leakage, we proposed that the role of BiP in limiting Ca^{2+} leakage from the ER at the level of the Sec61 complex contributes to the connection between ER protein misfolding and apoptosis; misfolding polypeptides sequester BiP (in the absence of BiP, Sec61 complexes become leaky for Ca^{2+}), and Ca^{2+} transmission to mitochondria triggers apoptosis. This view was already partially confirmed (53). Furthermore, this notion is consistent with the observations that apoptosis can also be induced in HeLa cells by an inhibitor of CaM (70) and that *BIP* overexpression can protect cells from ER stress-associated cell death (71). This concept was further strengthened by the observations that the BiP co-chaperones ERj3 and ERj6 support BiP in Sec61 channel closure (Figs. 2 and 4) and that loss of ERj6 function in mice and humans also causes pancreatic β-cell apoptosis and diabetes (20, 64). The observation that loss of ERj4 function also leads to pancreatic β-cell apoptosis and diabetes may indicate that under stress conditions, ERj4 may be an additional co-chaperone for BiP in Sec61 channel closure (21). On this basis, we propose that a contribution of ER Ca^{2+} leakage to the shift to apoptosis is particularly significant in cell types with high protein secretion activity. These are cells with extensive rough ER and a high Sec61 content, such as pancreatic β-cells and hepatocytes, and depend on BiP, ERj3, and ERj6 to limit ER Ca^{2+} leakage. We suggest the term "Sec61 channelopathies" for diseases with an altered Sec61 channel function that is due to either subunits of the Sec61 complex or direct or indirect effectors thereof, such as BiP and its co-chaperones. Examples of such diseases are certain forms of diabetes in mice and humans, polycystic liver disease in humans and mice, and hemolytic uremic syndrome in humans (Table 2). We note that there is also a human hereditary disease that is caused by apoptosis and relates to the level of available BiP, the neurodegenerative Marinesco-Sjögren syndrome (72). In this case, the mutated gene

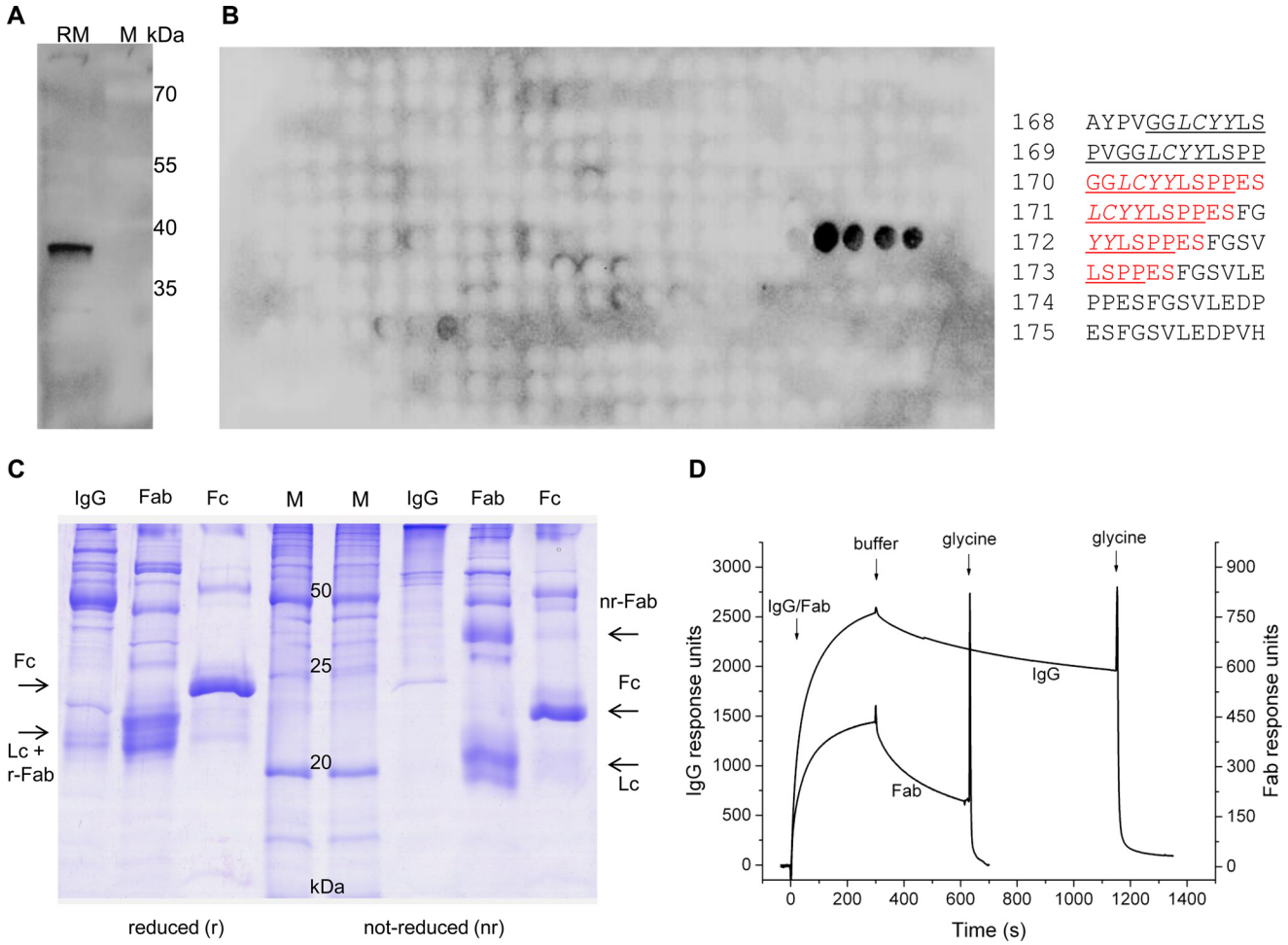

FIGURE 10. **Purification and characterization of anti-loop 7 antibodies and Fabs.** *A*, canine pancreatic rough microsomes (*RM*) were subjected to SDS-PAGE in parallel to molecular mass standards (*M*) and blotted to PVDF membranes. The loop 7-specific rabbit polyclonal antibody was used as well as a secondary POD-coupled anti-rabbit antibody and ECL™ for visualization with a Fusion SL luminescence imaging system. *B*, peptide spot array of Sec61α (corresponding to the complete amino acid sequence 12 amino acid residues in length with a shift of two amino acids) was incubated with affinity-purified anti-loop 7 IgGs and, thereafter, visualized by anti-rabbit-POD and ECL. Only the peptide epitope (residues 339–353) showed signals for antibody binding. The peptide numbers are given as well as their corresponding sequences; the positive peptides are indicated by *red type* for the amino acid residues that were used for immunization. The BiP binding site is *underlined*, and the minihelix is given in *italic type* (16). *C*, Fab production from affinity-purified IgGs was evaluated by reductive and non-reductive SDS-PAGE. Coomassie staining of the resulting protein composition revealed the correct and efficient fragmentation of the IgGs by papain. *D*, IgG and Fab binding was evaluated in surface plasmon resonance experiments with immobilized peptide from loop 7 (residues 339–353) (measuring cell) and peptide 325–339 (control cell), respectively. Bound antibodies were released from peptides by application of 100 mM glycine/HCl (pH 2.8).

encodes the BiP-nucleotide exchange factor, termed Sil1, and the disease phenotype is most evident in Purkinje cells of the cerebellum. Of further note, too much suppression of ER Ca^{2+} leakage can also cause disease, such as cancers of the prostate and the lung, which are linked to overexpression of the *SEC62* gene (18). The corresponding protein is involved in CaM-mediated Sec61 channel closure (Fig. 1).

Author Contributions—S. S., M. C. K., and I. G. carried out the Ca^{2+} imaging experiments under the supervision of A. C. A. M. purified proteins and performed the Biacore experiments under the supervision of M. J. Q. W. and N. S. performed the co-IP experiments under the supervision of X. Z. C. B. H. and R. W. contributed the single channel measurements. S. S. did three-dimensional SIM and performed the quantitative PCR experiments with help from F. B. and M. G. P. L., S. U., and M. G. studied cell proliferation in real time and cell migration. S. H. carried out the protein transport experiments. J. D. supervised all cloning work and silencing experiments. M. J. purified, characterized, and used the anti-loop 7 antibodies in pull-down experiments. A. C. and R. Z. planned and supervised the project and wrote the manuscript together with S. S. All authors reviewed the results and approved the final version of the manuscript.

Acknowledgments—The D1ER expression plasmid was kindly provided by Dr. Roger Y. Tsien (University of California, San Diego, CA). Antibodies against ERj4 were kindly donated by Dr. L. Hendershot, and antibodies against ERj5 were kindly donated by Dr. G. Spyrou (Karolinska Institute, Stockholm, Sweden). We gratefully acknowledge the three-dimensional SIM supervision by Drs. E. Krause and J. Rettig (Saarland University, Homburg, Germany) and the expert technical assistance by M. Lerner, N. Heim, H. Löhr, and M. Simon Thomas (Saarland University, Homburg, Germany).

References

1. Blobel, G., and Dobberstein, B. (1975) Transfer of proteins across membranes. I. Presence of proteolytically processed and unprocessed nascent immunoglobulin light chains on membrane-bound ribosomes of murine myeloma. *J. Cell Biol.* **67,** 835–851

2. Crowley, K. S., Liao, S., Worrell, V. E., Reinhart, G. D., and Johnson, A. E. (1994) Secretory proteins move through the endoplasmic reticulum membrane via an aqueous, gated pore. *Cell* **78,** 461–471
3. Berridge, M. J. (2002) The endoplasmic reticulum: a multifunctional signalling organelle. *Cell Calcium* **32,** 235–249
4. Rizzuto, R., and Pozzan, T. (2006) Microdomains of intracellular Ca^{2+}: molecular determinants and functional consequences. *Physiol. Rev.* **86,** 369–408
5. Görlich, D., and Rapoport, T. A. (1993) Protein translocation into proteoliposomes reconstituted from purified components of the endoplasmic reticulum membrane. *Cell* **75,** 615–630
6. Hartmann, E., Sommer, T., Prehn, S., Görlich, D., Jentsch, S., and Rapoport, T. A. (1994) Evolutionary conservation of components of the protein translocation complex. *Nature* **367,** 654–657
7. Hamman, B. D., Chen, J. C., Johnson, E. E., and Johnson, A. E. (1997) The aqueous pore through the translocon has a diameter of 40–60 Å during cotranslational protein translocation at the ER membrane. *Cell* **89,** 535–544
8. Hamman, B. D., Hendershot, L. M., and Johnson, A. E. (1998) BiP maintains the permeability barrier of the ER membrane by sealing the lumenal end of the translocon pore before and early in translocation. *Cell* **92,** 747–758
9. Wirth, A., Jung, M., Bies, C., Frien, M., Tyedmers, J., Zimmermann, R., and Wagner, R. (2003) The Sec61p complex is a dynamic precursor activated channel. *Mol. Cell* **12,** 261–268
10. Zimmermann, R., Eyrisch, S., Ahmad, M., and Helms, V. (2011) Protein translocation across the ER membrane. *Biochim. Biophys. Acta* **1808,** 912–924
11. Dudek, J., Pfeffer, S., Lee, P.-H., Jung, M., Cavalié, A., Helms, V., Förster, F., and Zimmermann, R. (2015) Protein transport into the human endoplasmic reticulum. *J. Mol. Biol.* **427,** 1159–1175
12. Flourakis, M., Van Coppenolle, F., Lehen'kyi, V., Beck, B., Skryma, R., and Prevarskaya, N. (2006) Passive calcium leak via translocon is a first step for iPLA2-pathway regulated store operated channels activation. *FASEB J.* **20,** 1215–1217
13. Erdmann, F., Schäuble, N., Lang, S., Jung, M., Honigmann, A., Ahmad, M., Dudek, J., Benedix, J., Harsman, A., Kopp, A., Helms, V., Cavalié, A., Wagner, R., and Zimmermann, R. (2011) Interaction of calmodulin with Sec61a limits Ca^{2+} leakage from the endoplasmic reticulum. *EMBO J.* **30,** 17–31
14. Lang, S., Erdmann, F., Jung, M., Wagner, R., Cavalie, A., and Zimmermann, R. (2011) Sec61 complexes form ubiquitous ER Ca^{2+} leak channels. *Channels* **5,** 228–235
15. Camello, C., Lomax, R., Petersen, O. H., and Tepikin, A. V. (2002) Calcium leak from intracellular stores: the enigma of calcium signalling. *Cell Calcium* **32,** 355–361
16. Schäuble, N., Lang, S., Jung, M., Cappel, S., Schorr, S., Ulucan, Ö., Linxweiler, J., Dudek, J., Blum, R., Helms, V., Paton, A. W., Paton, J. C., Cavalié, A., and Zimmermann, R. (2012) BiP-mediated closing of the Sec61 channel limits Ca^{2+} leakage from the ER. *EMBO J.* **31,** 3282–3296
17. Alder, N. N., Shen, Y., Brodsky, J. L., Hendershot, L. M., and Johnson, A. E. (2005) The molecular mechanisms underlying BiP-mediated gating of the Sec61 translocon of the endoplasmic reticulum. *J. Cell Biol.* **168,** 389–399
18. Linxweiler, M., Schorr, S., Jung, M., Schäuble, N., Linxweiler, J., Langer, F., Schäfers, H.-J., Cavalié, A., Zimmermann, R., and Greiner, M. (2013) Targeting cell migration and the ER stress response with calmodulin antagonists: a clinically tested small molecule phenocopy of SEC62 gene silencing in human tumor cells. *BMC Cancer* **13,** 574
19. Lloyd, D. J., Wheeler, M. C., and Gekakis, N. (2010) A point mutation in Sec61α1 leads to diabetes and hepatosteatosis in mice. *Diabetes* **59,** 460–470
20. Ladiges, W. C., Knoblaugh, S. E., Morton, J. F., Korth, M. J., Sopher, B. L., Baskin, C. R., MacAuley, A., Goodman, A. G., LeBoeuf, R. C., and Katze, M. G. (2005) Pancreatic beta-cell failure and diabetes in mice with a deletion mutation of the endoplasmic reticulum molecular chaperone gene P58IPK. *Diabetes* **54,** 1074–1081
21. Fritz, J. M., Dong, M., Apsley, K. S., Martin, E. P., Na, C.-L., Sitaraman, S., and Weaver, T. E. (2014) Deficiency of the BiP cochaperone ERdj4 causes constitutive endoplasmic reticulum stress and metabolic defects. *Mol. Biol. Cell* **25,** 431–440
22. Harding, H. P., Zeng, H., Zhang, Y., Jungries, R., Chung, P., Plesken, H., Sabatini, D. D., and Ron, D. (2001) Diabetes mellitus and exocrine pancreatic dysfunction in $Perk^{-/-}$ mice reveals a role for translational control in secretory cell survival. *Mol. Cell* **7,** 1153–1163
23. Greiner, M., Kreutzer, B., Jung, V., Grobholz, R., Hasenfus, A., Stöhr, R. F., Franz, R., Tornillo, L., Dudek, J., Stöckle, M., Unteregger, G., Kamradt, J., Wullich, B., and Zimmermann, R. (2011) Silencing of the *SEC62* gene inhibits migratory and invasive potential of various tumor cells. *Int. J. Cancer* **128,** 2284–2295
24. Dudek, J., Greiner, M., Müller, A., Hendershot, L. M., Kopsch, K., Nastainczyk, W., and Zimmermann R. (2005) ERj1 plays a basic role in protein biogenesis at the endplasmic reticulum. *Nat. Struct. Mol. Biol.* **12,** 1008–1014
25. Tyedmers, J., Lerner, M., Bies, C., Dudek, J., Skowronek, M. H., Haas, I. G., Heim, N., Nastainczyk, W., Volkmer, J., and Zimmermann, R. (2000) Homologs of the yeast Sec complex subunits Sec62p and Sec63p are abundant proteins in dog pancreas microsomes. *Proc. Natl. Acad. Sci. U.S.A.* **97,** 7214–7219
26. Dudek, J., Volkmer, J., Bies, C., Guth, S., Müller, A., Lerner, M., Feick, P., Schäfer, K.-H., Morgenstern, E., Hennessy, F., Blatch, G. L., Janoscheck, K., Heim, N., Scholtes, P., Frien, M., Nastainczyk, W., and Zimmermann, R. (2002) A novel type of cochaperone mediates transmembrane recruitment of DnaK-like chaperones to ribosomes. *EMBO J.* **21,** 2958–2967
27. Weitzmann, A., Baldes, C., Dudek, J., and Zimmermann, R. (2007) The Hsp70-molecular chaperone network in the pancreatic endoplasmic reticulum: a quantitative approach. *FEBS J.* **274,** 5175–5187
28. Zahedi, R. P., Völzing, C., Schmitt, A., Frien, M., Jung, M., Dudek, J., Wortelkamp, S., Sickmann, A., and Zimmermann, R. (2009) Analysis of the membrane proteome of canine pancreatic rough microsomes identifies a novel Hsp40, termed ERj7. *Proteomics* **9,** 3463–3473
29. Palmer, A. E., and Tsien, R. Y. (2006) Measuring calcium signaling using genetically targetable fluorescent indicators. *Nat. Protoc.* **1,** 1057–1065
30. Lang, S., Schäuble, N., Cavalié, A., and Zimmermann, R. (2011) Live cell calcium imaging combined with siRNA mediated gene silencing identifies Ca^{2+} leak channels in the ER membrane and their regulatory mechanisms. *J. Vis. Exp.* **53,** e2730
31. DuRose, J. B., Tam, A. B., and Niwa, M. (2006) Intrinsic capacities of molecular sensors of the unfolded protein response to sense alternate forms of endoplasmic reticulum stress. *Mol. Biol. Cell* **17,** 3095–3107
32. Johnson, N., Vilardi, F., Lang, S., Leznicki, P., Zimmermann, R., and High, S. (2012) TRC-40 can deliver short secretory proteins to the Sec61 translocon. *J. Cell Sci.* **125,** 3612–3620
33. Lang, S., Benedix, J., Fedeles, S. V., Schorr, S., Schirra, C., Schäuble, N., Jalal, C., Greiner, M., Hassdenteufel, S., Tatzelt, J., Kreutzer, B., Edelmann, L., Krause, E., Rettig, J., Somlo, S., Zimmermann, R., and Dudek, J. (2012) Different effects of Sec61a-, Sec62- and Sec63-depletion on transport of polypeptides into the endoplasmic reticulum of mammalian cells. *J. Cell Sci.* **125,** 1958–1969
34. Aneiros, E., Philipp, S., Lis, A., Freichel, M., and Cavalié, A. (2005) Modulation of Ca^{2+} signalling by Na^{+}/Ca^{2+} exchangers in mast cells. *J. Immunol.* **174,** 119–130
35. Gross, S. A., Guzmán, G. A., Wissenbach, U., Philipp, S. E., Zhu, M. X., Bruns, D., and Cavalié, A. (2009) TRPC5 is a Ca^{2+}-activated channel functionally coupled to Ca^{2+}-selective ion channels. *J. Biol. Chem.* **284,** 34423–34432
36. Grynkiewicz, G., Poenie, M., and Tsien, R. Y. (1985) A new generation of Ca^{2+} indicators with greatly improved fluorescence properties. *J. Biol. Chem.* **260,** 3440–3450
37. Yang, J., Wang, Q., Zheng, W., Tuli, J., Li, Q., Wu, Y., Hussein, S., Dai, X. Q., Shafiei, S., Li, X. G., Shen, P. Y., Tu, J. C., and Chen, X.-Z. (2012) Receptor for activated C kinase 1 (RACK1) inhibits function of transient receptor potential (TRP)-type channel Pkd2L1 through physical interaction. *J. Biol. Chem.* **287,** 6551–6561
38. Müller, P., Rudin, D., Tien, R., and Westcott, W. C. (1963) Methods for the formation of single bimolecular lipid membranes in aqueous solution. *J. Phys. Chem.* **67,** 534–535

39. Hilpert, K., Winkler, D. F., and Hancock, R. E. (2007) Peptide arrays on cellulose support: SPOT synthesis, a time and cost efficient method for synthesis of large numbers of peptides in a parallel and addressable fashion. *Nat. Protoc.* **2,** 1333–1349
40. Otero, J. H., Lizák, B., and Hendershot, L. M. (2010) Life and death of a BiP substrate. *Semin. Cell Dev. Biol.* **21,** 472–478
41. Melnyk, A., Rieger, H., and Zimmermann, R. (2015) Co-chaperones of the mammalian endoplasmic reticulum. *Subcell. Biochem.* **78,** 179–200
42. Brightman, S. E., Blatch, G. L., and Zetter, B. R. (1995) Isolation of a mouse cDNA encoding MTJ1, a new murine member of the DnaJ family of proteins. *Gene* **153,** 249–254
43. Mayer, H.-A., Grau, H., Kraft, R., Kosta, S., Prehn, S., Kalies, K.-U., and Hartmann, E. (2000) Mammalian Sec61 is associated with Sec62 and Sec63. *J. Biol. Chem.* **275,** 14550–14557
44. Bies, C., Guth, S., Janoschek, K., Nastainczyk, W., Volkmer, J., and Zimmermann, R. (1999) A Scj1p homolog and folding catalysts present in dog pancreas microsomes. *Biol. Chem.* **380,** 1175–1182
45. Shen, Y., Meunier, L., and Hendershot, L. M. (2002) Identification and characterization of a novel endoplasmic reticulum (ER) DnaJ homologue, which stimulates ATPase activity of BiP *in vitro* and is induced by ER stress. *J. Biol. Chem.* **277,** 15947–15956
46. Cunnea, P. M., Miranda-Vizuete, A., Bertoli, G., Simmen, T., Damdimopoulos, A. E., Hermann, S., Leinonen, S., Huikko, M. P., Gustafsson, J.-A., Sitia, R., and Spyrou, G. (2003) ERdj5, an endoplasmic reticulum (ER)-resident protein containing DnaJ and thioredoxin domains, is expressed in secretory cells or following ER stress. *J. Biol. Chem.* **278,** 1059–1066
47. Hosoda, A., Kimata, Y., Tsuru, A., and Kohno, K. (2003) JPDI, a novel endoplasmic reticulum-resident protein containing both a BiP-interacting J-domain and thioredoxin-like motifs. *J. Biol. Chem.* **278,** 2669–2676
48. Rutkowski, D. T., Kang, S. W., Goodman, A. G., Garrison, J. L., Taunton, J., Katze, M. G., Kaufman, R. J., and Hegde, R. S. (2007) The role of p58IPK in protecting the stressed endoplasmic reticulum. *Mol. Biol. Cell* **18,** 3681–3691
49. Petrova, K., Oyadomari, S., Hendershot, L. M., and Ron, D. (2008) Regulated association of misfolded endoplasmic reticulum lumenal proteins with P58/DNAJc3. *EMBO J.* **27,** 2862–2872
50. Oyadomari, S., Yun, C., Fisher, E. A., Kreglinger, N., Kreibich, G., Oyadomari, M., Harding, H. P., Goodman, A. G., Harant, H., Garrison, J. L., Taunton, J., Katze, M. G., and Ron, D. (2006) Cotranslocational degradation protects the stressed endoplasmic reticulum from protein overload. *Cell* **126,** 727–739
51. Dejgaard, K., Theberge, J.-F., Heath-Engel, H., Chevet, E., Tremblay, M. L., and Thomas, D. Y. (2010) Organization of the Sec61 translocon, studied by high resolution native electrophoresis. *J. Proteome Res.* **9,** 1763–1771
52. Williams, J. M., Inoue, T., Banks, L., and Tsai, B. (2013) The ERdj5-Sel1L complex facilitates cholera toxin retrotranslocation. *Mol. Biol. Cell* **24,** 785–795
53. Hammadi, M., Oulidi, A., Gackière, F., Katsogiannou, M., Slomianny, C., Roudbaraki, M., Dewailly, E., Delcourt, P., Lepage, G., Lotteau, S., Ducreux, S., Prevarskaya, N., and Van Coppenolle, F. (2013) Modulation of ER stress and apoptosis by endoplasmic reticulum calcium leak via translocon during unfolded protein response: involvement of GRP78. *FASEB J.* **27,** 1600–1609
54. Tsukazaki, T., Mori, H., Fukai, S., Ishitani, R., Mori, T., Dohmae, N., Perederina, A., Sugita, Y., Vassylyev, D. G., Ito, K., and Nureki, O. (2008) Conformational transition of Sec machinery inferred from bacterial SecYE structures. *Nature* **455,** 988–991
55. Linxweiler, M., Linxweiler, J., Barth, M., Benedix, J., Jung, V., Kim, Y.-J., Bohle, R. M., Zimmermann, R., and Greiner, M. (2012) Sec62 bridges the gap from 3q amplification to molecular cell biology in non-small cell lung cancer. *Am. J. Pathol.* **180,** 473–483
56. Lomax, R. B., Camello, C., Van Coppenolle, F., Petersen, O. H., Tepikin, A. V. (2002) Basal and physiological Ca^{2+} leak from the endoplasmic reticulum of pancreatic acinar cells: second messenger-activated channels and translocons. *J. Biol. Chem.* **277,** 26479–26485
57. Van Coppenolle, F., Vanden Abeele, F., Slomianny, C., Flourakis, M., Hesketh, J., Dewailly, E., and Prevarskaya, N. (2004) Ribosome-translocon complex mediates calcium leakage from endoplasmic reticulum stores. *J. Cell Sci.* **117,** 4135–4142
58. Giunti, R., Gamberucci, A., Fulceri, R., Bánhegyi, G., and Benedetti, A. (2007) Both translocon and a cation channel are involved in the passive Ca^{2+} leak from the endoplasmic reticulum: a mechanistic study on rat liver microsomes. *Arch. Biochem. Biophys.* **462,** 115–121
59. Ong, H. L., Liu, X., Sharma, A., Hegde, R. S., and Ambudkar, I. S. (2007) Intracellular Ca^{2+} release via the ER translocon activates store-operated calcium entry. *Pflugers Arch.* **453,** 797–808
60. Haigh, N. G., and Johnson, A. E. (2002) A new role for BiP: closing the aqueous translocon pore during protein integration into the ER membrane. *J. Cell Biol.* **156,** 261–270
61. Awad, W., Estrada, I., Shen, Y., and Hendershot, L. M. (2008) BiP mutants that are unable to interact with endoplasmic reticulum DnaJ proteins provide insight into interdomain interactions of BiP. *Proc. Natl. Acad. Sci. U.S.A.* **105,** 1164–1169
62. Bies, C., Blum, R., Dudek, J., Nastainczyk, W., Oberhauser, S., Jung, M., and Zimmermann, R. (2004) Characterization of pancreatic ERj3p, a homolog of yeast DnaJ-like protein Scj1p. *Biol. Chem.* **385,** 389–395
63. Shen, Y., and Hendershot, L. M. (2005) ERdj3p, a stress-inducible endoplasmic reticulum DnaJ homologue, serves as a cofactor for BiP's interactions with unfolded substrates. *Mol. Biol. Cell* **16,** 40–50
64. Synofzik, M., Haack, T. B., Kopajtich, R., Gorza, M., Rapaport, D., Greiner, M., Schönfeld, C., Freiberg, C., Schorr, S., Holl, R. W., Gonzalez, M. A., Fritsche, A., Fallier-Becker, P., Zimmermann, R., Strom, T. M., Meitinger, T., Züchner, S., Schüle, R., Schöls, L., and Prokisch, H. (2014) Absence of BiP co-chaperone DNAJC3 causes diabetes mellitus and multisystemic neurodegeneration. *Am. J. Hum. Genet.* **95,** 689–697
65. Davila, S., Furu, L., Gharavi, A. G., Tian, X., Onoe, T., Qian, Q., Li, A., Cai, Y., Kamath, P. S., King, B. F., Azurmendi, P. J., Tahvanainen, P., Kääriäinen, H., Höckerstedt, K., Devuyst, O., Pirson, Y., Martin, R. S., Lifton, R. P., Tahvanainen, E., Torres, V. E., and Somlo, S. (2004) Mutations in SEC63 cause autosomal dominant polycystic liver disease. *Nat. Genet.* **36,** 575–577
66. Fedeles, S. V., Tian, X., Gallagher, A.-R., Mitobe, M., Nishio, S., Lee, S. H., Cai, Y., Geng, L., Crews, C. M., and Somlo, S. (2011) A genetic interaction network of five genes for human polycystic kidney and liver disease defines polycystin-1 as the central determinant of cyst formation. *Nat. Genet.* **43,** 639–647
67. Marcinowski, M., Höller, M., Feige, M. J., Baerend, D., Lamb, D. C., and Buchner, J. (2011) Substrate discrimination of the chaperone BiP by autonomous and cochaperone-regulated conformational transitions. *Nat. Struct. Mol. Biol.* **18,** 150–158
68. Shore, G. C., Papa, F. R., and Oakes, S. A. (2011) Signaling cell death from the endoplasmic reticulum stress response. *Curr. Opin. Cell Biol.* **23,** 143–149
69. Schröder, M., and Kaufman, R. J. (2005) The mammalian unfolded protein response. *Annu. Rev. Biochem.* **74,** 739–789
70. Hu, Q., Chang, J., Tao, L., Yan, G., Xie, M., and Wang, Z. (2005) Endoplasmic reticulum mediated necrosis-like apoptosis of HeLa cells induced by Ca^{2+} oscillation. *J. Biochem. Mol. Biol.* **38,** 709–716
71. Suyama, K., Watanabe, M., Sakabe, K., Okada, Y., Matsuyama, D., Kuroiwa, M., and Mochida, J. (2011) Overexpression of GRP78 protects glial cells from endoplasmic reticulum stress. *Neurosci. Lett.* **504,** 271–276
72. Roos, A., Buchkremer, S., Kollipara, L., Labisch, T., Gatz, C., Zitzelsberger, M., Brauers, E., Nolte, K., Schröder, J. M., Kirschner, J., Jesse, C. M., Goebel, H. H., Goswami, A., Zimmermann, R., Zahedi, R. P., Senderek, J., and Weis, J. (2014) Myopathy in Marinesco-Sjögren syndrome links endoplasmic reticulum chaperone dysfunction to nuclear envelope pathology. *Acta Neuropathol.* **127,** 761–777